

Analyst

Accepted Manuscript

This article can be cited before page numbers have been issued, to do this please use: J. S. Sidhu, G. Kaur, A. R. Chavan, M. Chahal and R. Taliyan, *Analyst*, 2024, DOI: 10.1039/D4AN01082E.



This is an Accepted Manuscript, which has been through the Royal Society of Chemistry peer review process and has been accepted for publication.

Accepted Manuscripts are published online shortly after acceptance, before technical editing, formatting and proof reading. Using this free service, authors can make their results available to the community, in citable form, before we publish the edited article. We will replace this Accepted Manuscript with the edited and formatted Advance Article as soon as it is available.

You can find more information about Accepted Manuscripts in the [Information for Authors](#).

Please note that technical editing may introduce minor changes to the text and/or graphics, which may alter content. The journal's standard [Terms & Conditions](#) and the [Ethical guidelines](#) still apply. In no event shall the Royal Society of Chemistry be held responsible for any errors or omissions in this Accepted Manuscript or any consequences arising from the use of any information it contains.

Phenoxy-1,2-dioxetane-Based Activatable Chemiluminescent Probes: Tuning of Photophysical Properties for Tracing Enzymatic Activities in Living Cells

View Article Online
DOI: 10.1039/C4AN01082E

Jagpreet Singh Sidhu^{a*}, Gurjot Kaur^b, Atharva Rajesh Chavan^a, Mandeep K. Chahal^c and Rajeev Taliyan^a

^a Department of Pharmacy, Birla Institute of Technology and Science Pilani, Pilani Campus, Rajasthan, 333031, India

^b Khalsa College Amritsar, Punjab, 143002, India

^c School of Chemistry and Forensic Science, University of Kent, Canterbury, CT2 7NH, UK

*Email: jagpreet.sidhu@pilani.bits-pilani.ac.in

Abstract

The use of chemiluminophores for tracing enzymatic activities in live-cell imaging has gained significant attention, making them valuable tools for diagnostic applications. Among various chemiluminophores, the phenoxy-1,2-dioxetane scaffold exhibits significant structural versatility and its activation is governed by the Chemically Initiated Electron Exchange Luminescence (CIEEL) mechanism. This mechanism can be initiated by enzymatic activity, changes in pH, or other chemical stimuli. The photophysical properties of phenoxy-1,2-dioxetanes can be fine-tuned through the incorporation of different substituents on the phenolic ring and by anchoring them with specific triggers. This review discusses the variations in physicochemical properties, including emission maxima, quantum yield, aqueous solubility, and pKa, as influenced by structural modifications, thereby establishing a comprehensive structure-activity relationship. Furthermore, it categorises the probes based on different enzyme classes, such as hydrolase-sensitive probes, oxidoreductase-responsive probes, and transferase-activatable phenoxy-1,2-dioxetanes, offering a promising platform technology for the early diagnosis of diseases and disorders. The summary section highlights key opportunities and limitations associated with applying phenoxy-1,2-dioxetanes in achieving precise and effective enzyme assays.

Keywords: Phenoxy-1,2-dioxetane; Chemiluminescence; Enzyme; Diagnosis; *In-vivo* Imaging

1 Introduction

View Article Online
DOI: 10.1039/D4AN01082E

Activatable sensing systems have become increasingly prevalent in medical science to trace diverse bioinformatics in the context of location, time, and environment in living subjects.¹ Such systems are sensitive to external stimuli such as enzymes, biomolecules, or other cellular events and give the readout signal.² The “always on” sensing probes display unchanging optical signals in the presence or absence of target species and suffer from high background signals. On the contrary, activatable probe changes their output signal once they come in contact with the target of interest and thus provide a better signal-to-background ratio.^{3, 4} Optically detected chemical probes emerge as promising candidates for sensing and diagnosis due to their advantages, including high specificity, low detection thresholds, rapid response times, and straightforward technical implementation.^{5, 6} The last decade witnessed significant progress in cellular imaging techniques to reveal living cell secrets and disclose undiscovered disease information.^{7, 8} However, high energy from excitation sources causes permanent damage to living tissues, low signal-to-noise ratio, and autofluorescence background limit the applications of fluorescence-based sensors in clinical samples.^{9, 10} Moreover, the inadequate penetration of light in deep biological tissues primarily caused by scattering and absorption of high energy short waves is also a serious concern.^{11, 12} Unlike fluorescence, chemiluminescence is an optical imaging technique in which a luminophore generates light without requiring excitation energy from an external source.^{13, 14} It is a chemical reaction-based light emission phenomenon that can occur in a wide range of chemical events even inside living systems, where excited state intermediates subsequently break down to release the energy in the form of visible light.^{15, 16} The unique feature of chemiluminescence results in exceptional sensitivity by eliminating the need for excitation energy/source.¹⁷ As a result, it can mitigate the photobleaching, light scattering, background disturbance, and autofluorescence of biomolecules.^{18, 19} Thus, chemiluminescent probes have been actively explored for the non-invasive imaging of cellular events in living cells. Leveraging the potential of chemiluminescence, innovative imaging, and therapeutic approaches continue to emerge, necessitating a comprehensive and current assessment of advancements within this dynamic research domain.

The majority of these chemiluminescence probes are categorized into four groups:²⁰ 1. Luminol and its derivatives, 2. Cypridina luciferin derivatives, 3. Peroxyoxalate esters, and 4. phenoxy-1,2-dioxetanes (**Figure 1**). The luminescence of luminol and peroxyoxalate derivatives is generally triggered by oxidizing agents.^{21, 22} In such cases, the probe undergoes oxidation,

forming a highly energetic and unstable intermediate. Subsequently, the intermediate decomposes to generate luminogenic species that emit photons as it returns to its ground state.^{23, 24} These probes are commonly used for imaging hydrogen peroxide (H₂O₂) because it serves both as an oxidizing agent and as a target analyte in numerous research studies.^{25, 26} Furthermore, Cypridina-based chemiluminescent probes have been reported to be activated in the presence of singlet oxygen species.²⁷ As a result, most cypridina and luminol-based probes have been developed to trace cellular events linked to oxidizing species.²⁸ However, it is crucial to note that in addition to these analytes, enzymes play an extremely significant role in nearly every cellular pathway. Enzymes are ubiquitous polypeptide biomolecules that catalyse selective and specific biochemical reactions.^{29, 30} A diverse array of enzymes, including esterases, oxidases, reductases, proteases, and transferases are the key biocatalyst and central figures in the chemistry of living organisms. Their involvement ranges from facilitating abnormal cellular growth to triggering inflammatory responses to a diseased state.^{31, 32} Therefore, understanding the physiology of enzymes in disease pathogenesis offers invaluable insights for developing targeted therapeutic interventions and diagnostics. The disease diagnosis using enzyme triggering motif provides a promising approach to designing activatable probes. Presently, a plethora of enzyme-activatable optical probes have been documented.³³ In this regard, the luminescence properties of phenoxy-1,2-dioxetanes have been widely explored in the literature to facilitate the tracing of enzymatic activities.^{34, 35} Its luminescence properties can be tailored as per the specific enzyme's catalytic nature. Unlike other chemiluminophores, phenoxy-1,2-dioxetanes can be modified so that they get directly activated by the biochemical reactions of the enzymes without any assistance from oxidizing species.³⁶⁻³⁸ Interestingly, their emission has been controlled by shielding of phenolate with a protecting group, that can be only activated in an enzymatic event, therefore spontaneously initiating chemiluminescence.³⁹ For several decades, triggerable dioxetanes of this kind have been employed in commercially available *in-vitro* assays. Recently, there is a huge surge of research interest in the utilisation of chemiluminescent phenoxy-1,2-dioxetanes for *in-vivo* imaging, mainly due to their biocompatibility and potential to emit sufficiently bright light essential for live animal imaging.⁴⁰⁻⁴³

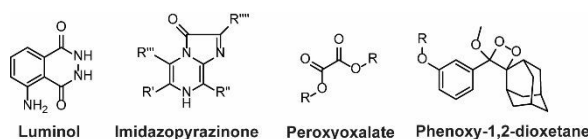


Figure 1: Chemical scaffolds of chemiluminescence probes.



Over the last decade, the structural properties of phenoxy-1,2-dioxetanes have been extensively explored through derivatisation with various functional groups. These structural changes result in fast chemo-excitation, pKa adjustment, improved quantum yields, and emission enhancement in physiological buffers.^{44, 45} As such, this review summarises the recent advancements in phenoxy-1,2-dioxetane derivatives tailored for monitoring enzymatic activities. It also explores the impact of different functional groups on their photophysical properties including emission maxima, quantum yields, and further outlines the designing principles of corresponding systems. Additionally, the review discusses potential challenges and outlines future directions for developing chemiluminescent technologies.

2 Photophysical and Structural Properties of Phenoxy-1,2-Dioxetanes

Over the years, phenoxy-1,2-dioxetanes have emerged as powerful light-emitting probes for bio-imaging applications, especially for activatable sensing.⁴⁶ The key advancement in the chemistry of these compounds occurred approximately three decades ago, marked by the Schaap group's discovery of triggerable dioxetanes.^{36, 37} Initial investigations revealed the involvement of phenoxy-1,2-dioxetane as an inherently unstable intermediate in numerous chemiluminescence systems.⁴⁷ Over time, certain phenoxy-1,2-dioxetanes are developed that can be selectively activated by a specific analyte of interest and result in chemiluminescence.^{41, 48, 49} The activation of the 1,2-dioxetane probe occurs via the Chemically Initiated Electron Exchange Luminescence (CIEEL) mechanism, where chemiexcitation is initiated through a phenolate-dioxetane biradical intermediates (**Figure 2**). These biradical intermediate undergoes further decomposition through the intramolecular back electron transfer (BET) mechanism and releases the energy to excite benzoate ester. Ultimately, it returns to the ground state and emits light of a specific wavelength.^{18, 50-54} Unlike conventional chemiluminophores, the chemiexcitation processes of phenoxy-1,2-dioxetanes rely not only on oxidative species, but enzymes can also trigger chemiluminescence.^{19, 55}

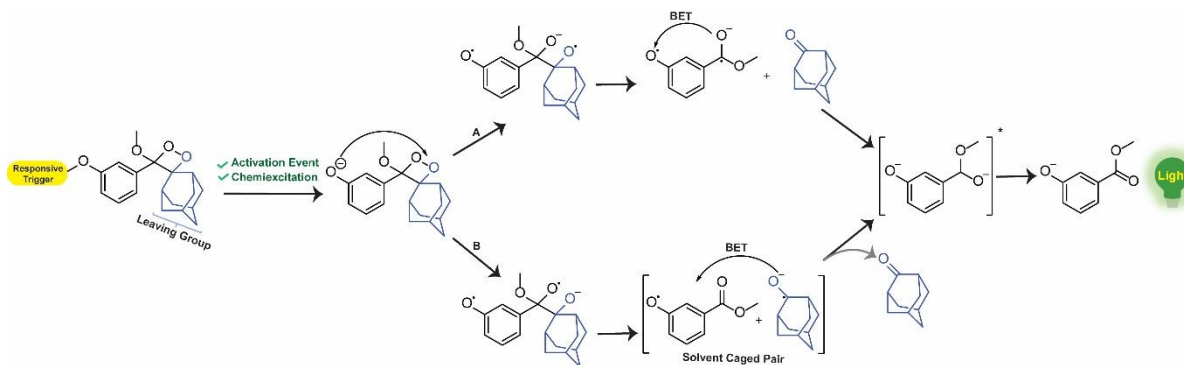


Figure 2: Chemiexcitation activation mechanism of phenoxy-1,2-dioxetane-based probes through CIELL. View Article Online
DOI: 10.1039/D4AN01082E

However, to activate first-generation phenoxy-1,2-dioxetane for chemiluminescence, a higher pH (approximately 10) was required, which hampered its applications for live animal imaging.⁵⁶ Hence, to decrease the pKa of phenol-dioxetane, Lippert and coworkers synthesised both halogenated and unsubstituted derivatives of phenoxy-1,2-dioxetane (**CL-1a**, **CL-1b**, and **CL-1c**).⁴¹ This work revealed that the acidity of phenol is increased due to the presence of *ortho* halogens and resulted in the highest chemiluminescence at pH 7.4, therefore confirming that lowering the pKa of phenol is accountable for enhancing chemiluminescence at physiological pH. Furthermore, to improve the chemiluminescence in an aqueous medium at neutral pH, Higuchi and coworkers introduced acetamide group *ortho* to phenol (**CL-2**).⁵⁷ **CL-2** is expected to have a lower pKa value due to intramolecular NH...O hydrogen bonding interactions in both neutral and anionic states. Recently, Pu and coworkers reported benzoxazole substituted phenoxy-1,2-dioxetane probes (**CL-3a** and **CL-3b**), to study the role of intramolecular hydrogen bonding in their chemiluminescence response.⁵⁸ They have found that the presence of benzoxazole moiety resulted in both increased chemiluminescence half-lives (up to ~33-fold) and 8.2-fold higher brightness in comparison to the classical methylacrylate-phenoxy-1,2-dioxetane derivative (**CL-4**) in aqueous solution. Although halogens and H-bonding groups containing probes were activatable at physiological pH in aqueous solution however, their chemiluminescence quantum yields were not improved significantly due to the quenching effect of water molecules. Shabat and coworkers have adopted multiple strategies to improve aqueous emission and quantum yield. They hypothesised that enhancement in quantum yield of phenoxy-1,2-dioxetane could be achieved by incorporating an electron acceptor, namely an acrylic ester/acrylonitrile group at *ortho* to phenolate donor.⁵⁹ To investigate the role of electron-withdrawing groups (EWGs), they have synthesised acryl-substituted phenoxy-benzoate derivatives, **CL-5** and **CL-6**.⁵⁹ The presence of EWGs significantly improved the emission in water, with Φ_{CL} (chemiluminescence quantum yield) values reaching up to 40% (Table 1). These findings suggested that the introduction of an acryl group into the phenoxy-1,2-dioxetane could elevate its Φ_{CL} under physiological conditions. Furthermore, replacing acryl ester and acrylonitrile with acrylic acid (**CL-5d**) substantially amplified the chemiexcitation rate in an aqueous solution. Additionally, the presence of chlorine at the *ortho* position reduced the pKa of phenolic OH, resulting in an enhanced extinction coefficient. The increase in extinction coefficient was attributed to the

higher concentration of the phenoxide ions in an aqueous medium induced by chlorine substituent. However, this alteration did not affect the emission wavelength and had a minor impact on the quantum yield. The improvement in the kinetic profile of luminophores is generally accompanied by a decrease in $T_{1/2}$ of luminophores (Table 1). In summary, the luminophores substituted with acryl-group (with or without chlorine) demonstrate notably intense chemiluminescent emission upon deprotonation at pH 7.4, with Φ_{CL} values reaching up to 3000 times over the unmodified structures.

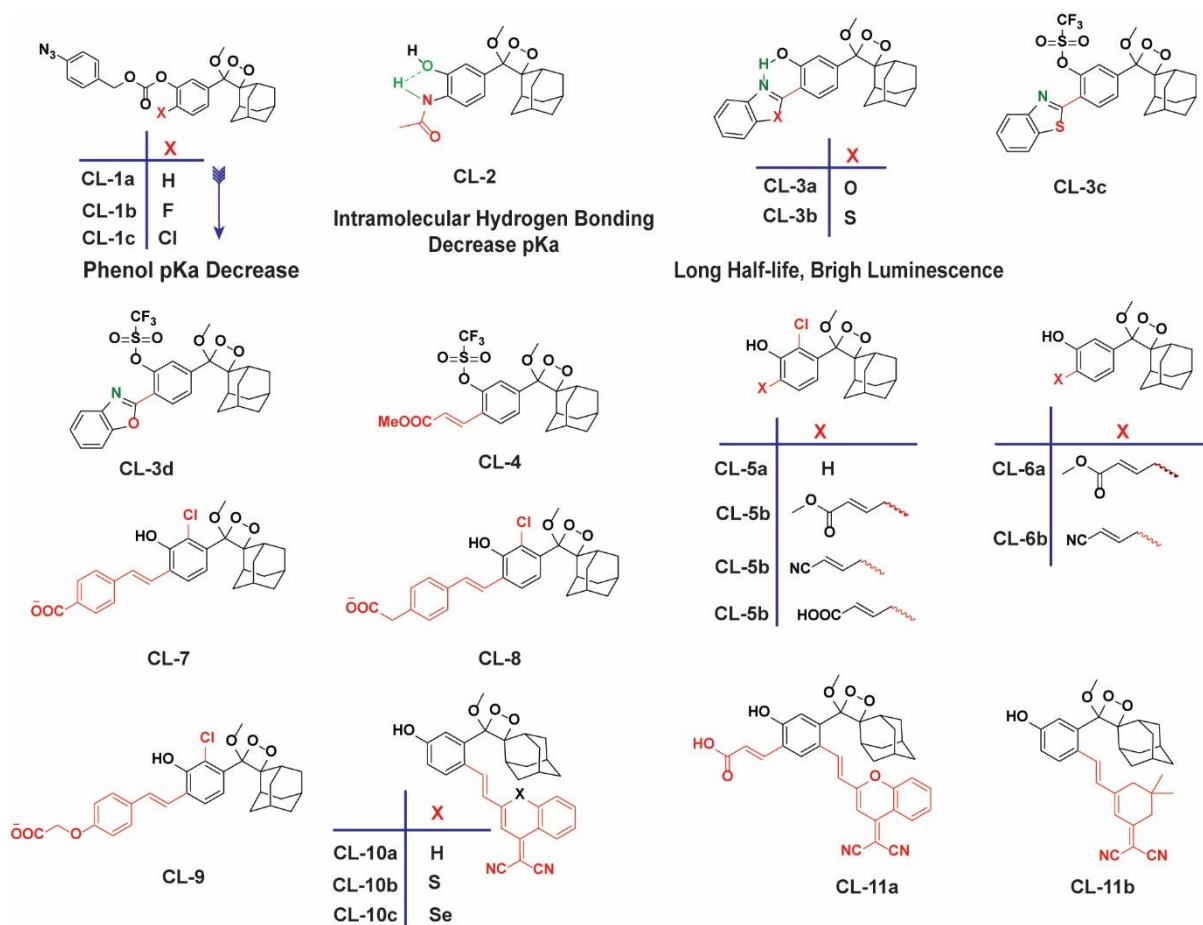


Figure 3: Chemical Structural Framework of Phenoxy-1,2-dioxetane derivatives (CL-1 to CL-11).

Further, in specific chemiluminescence bioassays, the absolute quantum yield of luminophore isn't the primary factor determining the efficacy of a chemiluminescent probe. Instead, what matters significantly is the rate at which chemiexcitation occurs within the free phenolate-dioxetane. Luminophores exhibiting rapid chemiexcitation kinetics are highly sought after because they have the potential to enhance the sensitivity of chemiluminescent analytical bioassays. A faster release of photons leads to a higher signal-to-noise ratio within a shorter timeframe, ultimately resulting in improved sensitivity. To improve the chemiexcitation rate,

Open Access Article. Published on 12/12/2024. Downloaded on 12/12/2024 09:14:20. This article is licensed under a Creative Commons Attribution-NonCommercial 3.0 Unported Licence.



Shabat and coworkers stabilised the phenoxy radical with styryl substituents (**CL-7**, **CL-8**, and **CL-9**).⁶⁰ The chemiexcitation of the styryl derivatives happened approximately at two orders of magnitude higher than the chemiexcitation of the **CL-5** and **CL-6**, as well as the unsubstituted Schaap's dioxetane (**CL-5a**). Further, the change in the pH did not affect the half-lives and thus proved that chemiexcitation is an intrinsic factor without any impact on pKa. With these structural modifications, the physicochemical properties of phenoxy-1,2-dioxetane derivatives were improved to visualise enzymatic activities in living cells. So, by considering all these parameters, the probes have been tailored for the sensing of enzymes, as discussed in the next section.

Table 1: Photo-physical Properties of **CL-1** to **CL-11**

Probe	λ_{\max} CL (nm)	$T_{1/2}$	Φ_{cl} ($\times 10^{-2}$ Einstein/mol)	Test Condition	Reference
CL-2	450	-	2.7×10^{-4}	pH 11.0	57
CL-3b	515	23.2 h	-	PBS (10% DMSO)	58
CL-3c	515	121 min	0.189	PBS (pH 7.4, 10% DMSO)	58
CL-3d	515	129 min	0.137	PBS (pH 7.4, 10% DMSO)	58
CL-4	515	3.6 min	0.023	PBS (pH 7.4, 10% DMSO)	58
CL-5a	470	17 min	0.003	PBS (pH 7.4, 5% DMSO)	11
CL-5b	540	~7 min	2.5	PBS (pH 7.4, 5% DMSO)	11
CL-5c	525	10 min	9.8	PBS (pH 7.4, 5% DMSO)	
CL-5d	510	85 s	0.098	in PBS (10% DMSO)	
CL-6a	540	23 min	2.3	PBS (pH 7.4, 5% DMSO)	
CL-6b	525	22 min	7.4	PBS (pH 7.4, 5% DMSO)	
CL-7	535	8.4 s	4.2	PBS (pH 7.4, 10 % DMSO)	60
CL-8	500	5.1 s	1.4	PBS (pH 7.4, 10 % DMSO)	60
CL-9	490	3.2 s	0.6	PBS (pH 7.4, 10 % DMSO)	60
CL-10a	660	178 min	0.82	PBS (pH 7.4, 10% FBS)	61

CL-10b	760	-	0.23	PBS (pH 7.4, 1% DMSO)	62
CL-10c	780	-	0.12	PBS (pH 7.4, 1% DMSO)	62
CL-11a	690	53 min	1.125	PBS (pH 7.4, 10% FBS)	61
CL-11b	650	14 min	2.90	PBS (10% DMSO)	63

To employ Schaap's dioxetanes for live-cell imaging, it is crucial to enhance the aqueous solubility and adjust their light emission towards the near-infrared (NIR) region. NIR wavelengths are highly advantageous for live imaging as they can penetrate deeply into tissues and encounter less scattering than shorter wavelengths.^{64, 65} In live-cell imaging direction, Shabat and coworkers conjugated dicyanomethylene-4H-chromene (DCMC) at the *para* position of phenol donor in phenoxy-dioxetane probe (**CL-10a**) that resulted in NIR-emission at 660 nm with comparative quantum yield.⁶¹ A particularly remarkable luminophore that possesses a DCMC acceptor along with an acrylic acid substituent at the *ortho* position of the phenol (**CL-11a**) exhibited a faster kinetic ($T_{1/2}$ 53 minutes) profile than **CL-10a** ($T_{1/2}$ 178 minutes). Faster kinetic is attributed to lower pKa of phenol, which ultimately affects the generation of phenolate species. Additionally, substituting oxygen atom with sulfur in the dicyanomethylene-4H-chromene ring (**CL-10b**) leads to improvement both in NIR emission (760 nm) and also chemiluminescence quantum yield (Table 1). Interestingly, the substitution of sulfur with selenium (**CL-10c**) further increased the emission wavelength (780 nm); however, it compromised with Φ_{CL} (0.12×10^{-2} Einstein/mol). The increment in emission energy was explained based on a decrease in the energy gap between the ground and the excited state of the molecule. Among the three hetero atoms, the inclusion of sulfur exhibited the brightest chemiluminescence and the highest signal-to-background ratio (SBR), approximately 415.1. Further, the conjugation of 2-(3,5,5-trimethylcyclohex-2-en-1-ylidene)malononitrile to phenoxy-1,2-dioxetane (**CL-11b**) compromised the emission wavelength (650 nm) but better Φ_{CL} (4.6×10^{-2} Einstein/mol) than **CL-11a**.⁶³ Thereby, it is worth playing around with extended π -conjugation in the molecular structure of phenoxy-1,2-dioxetanes for tuning the spectroscopic parameters (**Figure 3**). The chemiluminescence spectroscopic data of phenoxy-1,2-dioxetanes is summarised in Table 1. The molecular structures and chemiluminescence parameters of phenoxy-1,2-dioxetanes with different *ortho* substituents, are summarised in Table 2. Based on the photophysical properties and the chemical nature of the chemiluminophores, the structure-activity relationship has been drawn in **Figure 4**.

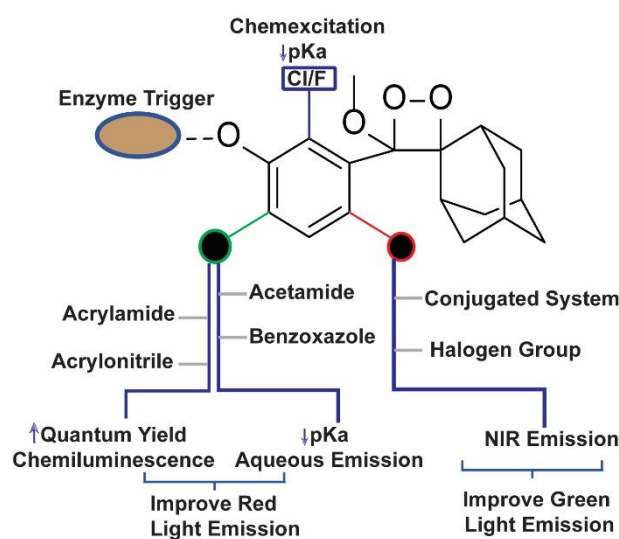
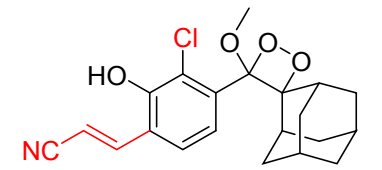
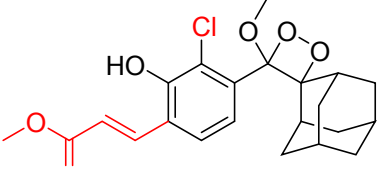
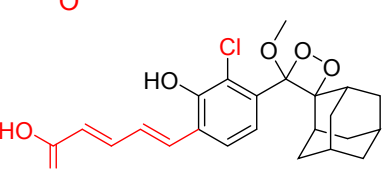
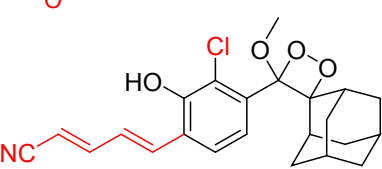
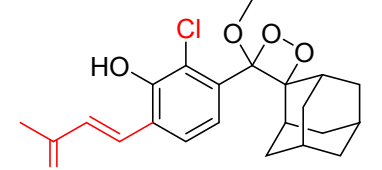
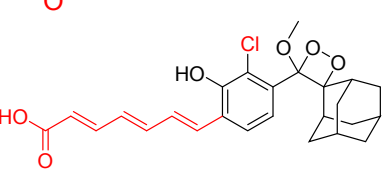
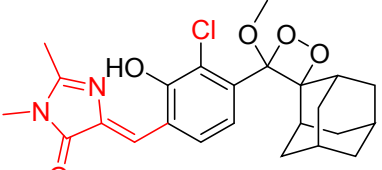
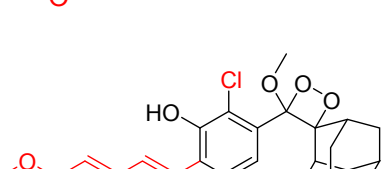
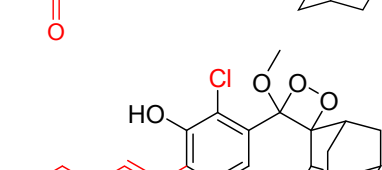


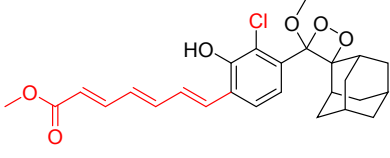
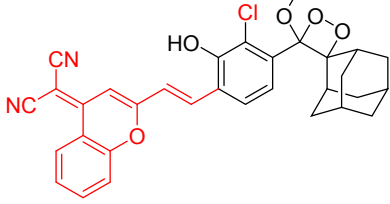
Figure 4: Structure-Activity Relationship of Phenoxy-1,2-dioxetane to tune Physico-chemical Parameters.

Table 2: Spectroscopic Parameters of Phenoxy 1,2-dioxetane Derivatives in PBS (100mM), pH 7.4, 10% DMSO.⁴³

Phenoxy 1,2-dioxetane	λ_{\max} CL [nm]	$T_{1/2}$	Relative Brightness	Φ CL %
	460 nm	16 hours	1	55
	490 nm	10.3 hours	0.70	20
	495 nm	3.4 s	480	0.58
	510 nm	1.6 min	245	9.8

	520 nm	20 min	41	20
	550 nm	10.5 min	16	4.8
	540 nm	15.6 s	206	1.9
	590 nm	2 min	39	1.1
	600 nm	13.5 min	0.85	0.42
	600 nm	3.3 s	65	0.14
	610 nm	11.9 min	0.25	0.073
	610 nm	31.2 s	8.3	0.5
	660 nm	5 min	0.24	0.13

View Article Online
DOI: 10.1039/D4AN01082E

				View Article Online DOI: 10.1039/D4AN01082E
	670 nm	18 s	1.2	0.012
	710 nm	17 min	0.61	0.38

3 Enzyme Triggered Phenoxy-1,2-Dioxetane

3.1 Hydrolase Selective Chemiluminescence Probe

Fibroblast Activation Protein-alpha (FAP α): FAP α (EC3.4.21.B28) is a transmembrane type

II serine proteolytic enzymes that participate in the hydrolysis of the peptide bonds and are involved in multiple pathogenesis, including cancer.^{66, 67} It possesses the capability to break down various components of the extracellular matrix (ECM) and has dipeptidyl peptidase (DPP) activity. Degradation of ECM is a key component in influencing the growth, invasion, and metastasis of tumors. It is also implicated in the excessive growth observed in the boundaries of keloid wounds and contributes to the invasive nature of keloids.^{68, 69} Therefore, tracing of FAP α activity holds significant importance in disease diagnosis. Recently, Ca and coworkers developed the first phenoxy-1,2-dioxetane-based chemiluminescence probes (**CL-12a**, **CL-12b**, and **CL-12c**) bearing acrylic ester and chlorine group *ortho* to phenol for the detection of FAP α .⁷⁰ The phenolic OH was masked with glycine-proline dipeptide to restrain the chemiexcitation of luminophore. FAP α hydrolysed peptide bond after proline, forming phenoxy-dioxetane (through 1,6 elimination rearrangement) that rapidly decomposes *via* CIEEL process to excited benzoate ester, which decayed to ground state with the release of green light energy. The results suggested that probes exhibited highly selective and sensitive detection of FAP α with a limit of detection 0.785, 0.965, and 0.587 ng/mL, using **CL-12a**, **CL-12b**, and **CL-12c**, respectively. Among all the probes, **CL-12a** showed the highest selectivity with 33 and 121-fold emission enhancement to FAP α over structurally similar enzymes - PREP

(prolyl oligopeptidase) and DPIV (dipeptidase IV), respectively. While **CL-12b** and **CL-12c** remained moderate to weak selective, which might be due to the inappropriate interactions of the probe at the active pocket of the enzyme. Subsequently, the stronger chemiluminescent signal in the cytoplasm of **CL-12a** treated HepG2 cells compared to LO2 cells indicated higher expression of FAP α in cancerous cells than healthy ones (**Figure 5A**). The selectivity of probes for endogenous enzymes was analysed by treating the cell lines with different concentrations of FAP α inhibitor (SP-13786). Furthermore, **CL-12a** was directly injected into the tumor and also injected into the tumor pre-treated with FAP α inhibitor (**Figure 5B**). The higher chemiluminescence reported in the tumor site also proved the selectivity for endogenous FAP α and its applications for visualization of cancer cells.

Granzyme B: It is a type of serine protease releases into cancer cells by natural killer cells to triggers apoptotic cell death.⁷¹⁻⁷³ Through its proteolytic activity, Granzyme B targets various intracellular proteins involved in apoptotic signalling pathways, ultimately dismantling the target cells. Recent studies provided insights into the multifaceted roles of Granzyme B in immune regulation, inflammation, and tissue homeostasis.⁷⁴ To assay this enzyme, a probe (**CL-13**) was designed and synthesised by Vendrell and coworkers.⁷¹ **CL-13** was meticulously crafted to target Granzyme B with utmost precision and superior signal clarity amidst background noise. The probe comprises a phenolic hydroxyl group linked to Ile-Glu-Pro-Asp peptide through a self-immolating linker. The authors has found that within 10 minutes of incubation of **CL-13** with Granzyme B led to cleavage of peptide linkage accompanied by 139-fold chemiluminescence enhancement at 520 nm. The varying concentrations of Granzyme B showed linear enhancement in chemiluminescence with a detection limit of 0.7 nM. Furthermore, as shown in **Figure 5C**, bright emission in MDA-MB cells co-cultured with NK cells as opposed to MDA-MB-231 signified the higher expression of Granzyme B in NK cells. Subsequently, **CL-13** was administered into the tumor contained NK cells, and live animal images were recorded immediately (**Figure 5D**). Bright chemiluminescent signals were reported exclusively in the tumor area administered with NK cells injection.



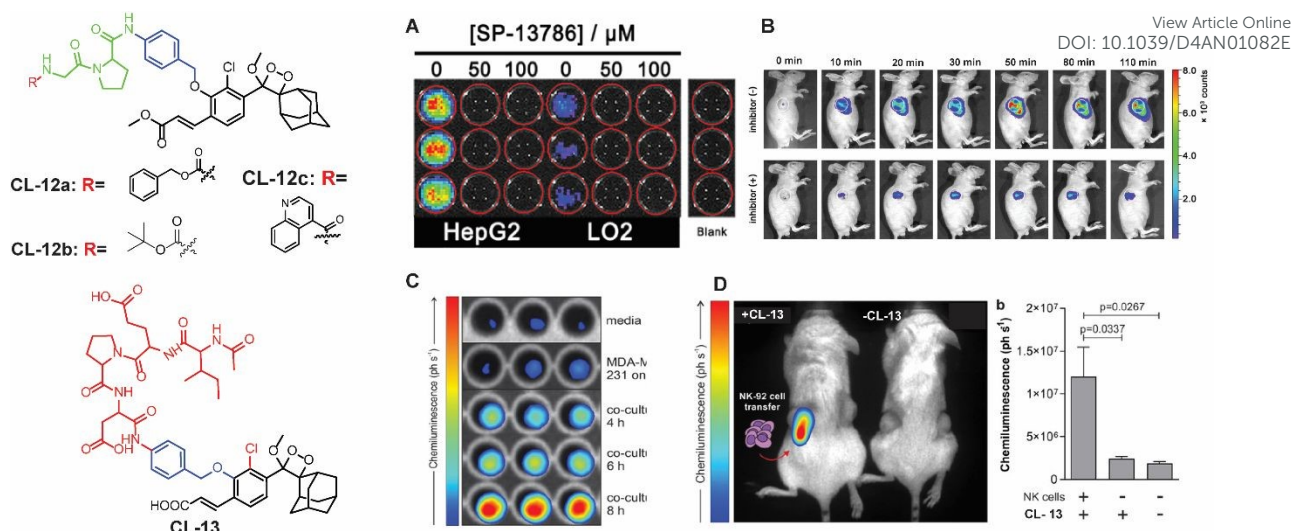


Figure 5: Molecular structure of CL-12 and CL-13 (A) Chemiluminescence images of HepG2 and LO2 upon treatment with CL-12a. (B) Chemiluminescence response of CL-12 in animal models at different time intervals with and without inhibitor. (C) Chemiluminescence images of CL-13 incubated with media only, MDA-MB-231 cells alone, and co-cultures of MDA-MB-231 cells with NK-92 cells for indicated times. (D) Chemiluminescence quantification in animal models. Figures A and B are reproduced with permission.⁷⁰ Copyright © 2021 American Chemical Society. C and D reprinted with permission.⁷¹ Copyright 2021 Wiley-VCH.

Aminopeptidases

Aminopeptidase N (APN; EC 3.4.11.2): It is an extracellular protease enzyme entails the cleavage of amino acid residues from the N-terminal of a substrate.⁷⁵ It is a widely distributed transmembrane ectoenzyme, participating in various physiological events, including cell migration, cell survival, angiogenesis, and viral uptake.⁷⁶ It is a well-known biomarker of hematopoietic cells, and elevated expression facilitates tumor cell invasion.⁷⁷ The correlation between its expression levels and invasive capacity underscores APN's potential as a therapeutic target for cancer pathogenesis and its diagnosis.⁷⁸ Recently, numerous activatable chemiluminescence strategies have been adopted for monitoring APN activities. Lian and coworkers constructed APN-triggered phenoxy-1,2-dioxetane derivative probe, CL-14.⁷⁹ The native chemiluminescence of the phenoxy-1,2-dioxetane nucleus was quenched by masking phenolic OH with L-alanine motif through *para*-amino benzyl alcohol as a self-immolative linker. The probe was also decorated with acrylonitrile group *ortho* to phenol to improve quantum yield and luminous time. Once hydrolysed by APN, the probe was rapidly activated and showed 26-fold chemiluminescence enhancement with a detection limit of 0.53 ng/mL. Chemiluminescence signals linearly correlated to cell densities of HepG-2 in the range of



0.2×10⁴ to 2.0×10⁴. The primary approach to treat malignancies is through surgical procedures, which often provide the most effective chance for cure in many cases. The success of the surgery depends on the thoroughness of identifying and removing all aspects of the tumor, including its borders, microscopic elements, and any metastatic lesions. If the surgical resection is incomplete, there's a risk of the malignant tumors recurring. In this particular report, probe solution was sprayed around the tumor for *in situ* tumor imaging. The chemiluminescence emission within the tumor tissue in animal models rose quickly, with a tumor-to-normal tissue ratio of 1.2 × 10⁶ being recorded (**Figure 6A**) followed by image-guided surgical removal of tumor tissue ensured complete excision for cancerous cells (**Figure 6B**). Instead of acrylonitrile, Gao and coworkers reported an acrylic ester-based chemiluminescence probe (**CL-15**) for image-guided tumor surgery.⁸⁰ It showed almost 190-fold chemiluminescence enhancement at 540 nm within 20 minutes of co-existence with APN. Moreover, the LOD (0.056 ng/mL) showed almost ten times higher sensitivity than **CL-14**. The chemiluminescence signal was detectable even at 20 mm thickness of chicken breast tissues with an extremely low background signal (174.2 ± 30.2). Therefore, **CL-15** was employed to distinguish tumor tissues from normal ones by directly spraying its aqueous solution on HepG2 xenograft tumors *ex vivo*, with normal liver tissues as controls. It exhibited a high tumor-to-normal tissue ratio (T/N 160), which might be a promising approach for precise tumor resection. In an orthotopic HepG2-tumor mice model, a luminescent signal reached a maximum within 10 minutes post-injection at the tumor site and lasting over 40 minutes (**Figure 6C and 6D**) may facilitate the removal of identified tumors under chemiluminescence guidance. Furthermore, Cao and coworkers replaced alanine with leucine to switch off the chemiexcitation and thus developed the **CL-16** probe.⁸¹ It showed 53-fold emission enhancement upon incubation with APN, and the detection limit was reported as 0.068 U/mL. Cellular studies revealed that the probe is permeable through the cell membrane and chemiluminescence switched on in response to endogenous APN. The probe solution when injected into the tumor area showed a drastic increase in chemiluminescence intensity within 5 minutes of incubation and attained saturation in 20 minutes, while the tumor treated with an APN inhibitor did not show any noticeable emission. Based on the structure of these probes, we conclude that the presence of acrylic ester instead of acrylonitrile group improved the detection limit with a better signal-to-noise ratio. It might be due to the more hydrophobic nature of acrylic ester than acrylic acid facilitated the cell membrane permeability.



Leucine Amino Peptidase (LAP): LAP (EC 3.4.11.1) is a proteolytic enzyme that belongs to M1 and M17 peptidase, which catalyses the cleavage of the peptide bond between the N-termini leucine residue in proteins.⁸² Understanding LAP's enzymatic activity is crucial for elucidating its role in physiological processes and exploring its potential as a target for therapeutic intervention in diseases where dysregulation of peptide metabolism is implicated. Cheng and coworkers explored chemiluminescence probes (**CL-17a** and **CL-17b**) that incorporated l-leucine into phenoxy-1,2-dioxetane to target LAP.⁸³ *In-vivo* imaging is preferably achieved using NIR chemiluminescence emission because of its superior depth penetration, **CL-17b** behaves as NIR chemiluminescence as π -electron system of the phenolic luminophore has been extended by inserting dicyano methyl chromone *ortho* to phenol. The luminescence of the **CL-17a** (conventional probe) attained emission saturation at 550 nm within 20 minutes of LAP catalytic action. However, NIR emitting **CL-17b** remained inactive under similar conditions. Computational studies demonstrated that **CL-17b** faced steric hindrance in reaching the enzyme's active site due to its larger size, while **CL-17a** interacts through hydrogen bonding and thus is catalysed by LAP. It showed a signal-to-noise value of approximately 1260 with a detection limit of 0.008 U/mL. The higher chemiluminescence signal of HePG-2 cells compared to LO2 cells upon treatment with CL-17a justified the application for the differentiation of cancer cells from normal ones. Saturation in chemiluminescence signal after 10 minutes of injection into the tumor has also been reported by authors. The selectivity of the probe was predicted by inhibiting the LAP activity with Ube, followed by **CL-17a** treatment (**Figure 5E**). Furthermore, cancerous liver tissue showed higher chemiluminescence intensity than normal ones establishing the application potential of **CL-17a** for detection of LAP in clinical samples.

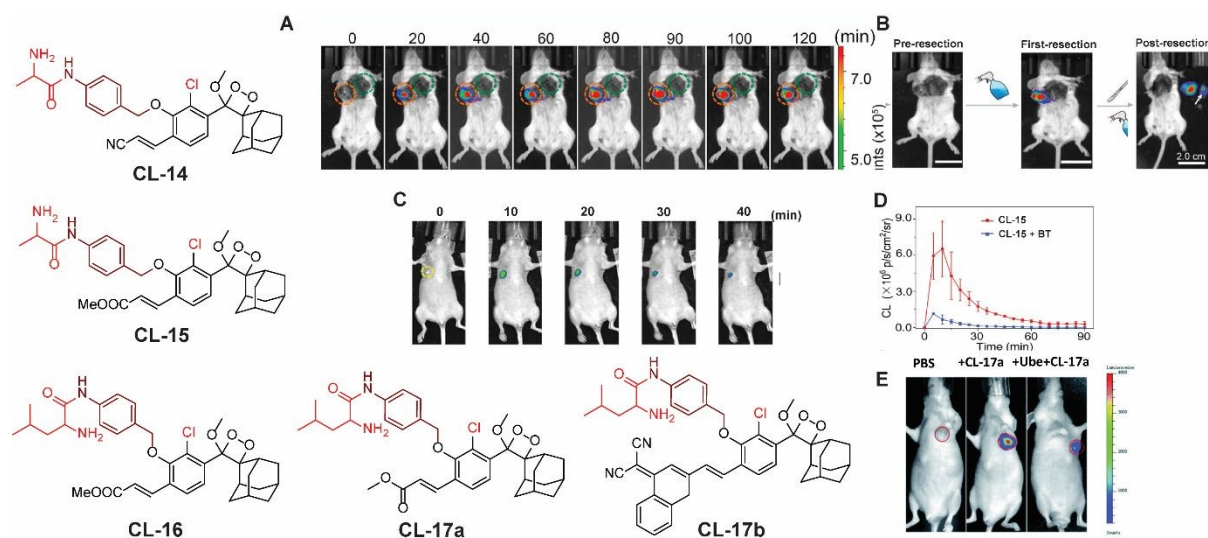


Figure 6: Chemiluminescence probes (CL- 14 to CL- 17b) for Aminopeptidase N and Leucine Aminopeptidase (A) Chemiluminescence images of 4T1-tumor-mice after spraying of **CL-14** (B) Image-guided tumor surgery using **CL-14**. Reprinted with permission.⁷⁹ Copyright 2022 Elsevier B.V. (C) Chemiluminescence Image of HepG2 xenograft after intra-tumoral injection of **CL-15**. (D) Quantification of chemiluminescence signal of **CL-15**. (E) Live animal images of HepG2 tumor-containing mice. C and D reprinted with permission.⁸⁰ Copyright 2022 Wiley-VCH GmbH. Figure E is reproduced from reference ⁸³ with permission from the Royal Society of Chemistry. Copyright © 2022 Royal Society of Chemistry.

Prostate-specific antigen (PSA, EC 3.4. 21.77): It is a serine protease enzyme hydrolyses the amide linkage of peptide substrate after glutamine. It is a key biomarker in the realm of prostate cancer diagnosis, prognosis, and therapeutic monitoring.^{84, 85} Initially, it was identified for its role in liquefying seminal fluid but later garnered widespread attention due to its remarkable specificity to the prostate gland. Over the years, PSA has transitioned from a mere physiological marker to a crucial tool in the early detection of prostate cancer and semen analysis in criminal cases.⁸⁶ To target PSA, Portnoy and coworkers employed Mu-HSSKLQ polypeptide, as a PSA trigger.⁸⁷ The chemiluminescence of *ortho* acrylic acid substituted phenoxy-1,2-dioxetane quenched with said peptide (**CL-18**). The cleavage of peptide bonds in the presence of PSA has led to a 157-fold change in emission intensity and 63-fold higher signal-to-noise ratio achieved as compared to a commercially available fluorescent probe. It distinctly underscores the superior PSA-detection capability of CL-18 over fluorescence ones. The real-time semen samples showed 14-fold chemiluminescence compared to the control. Furthermore, the probe maintained its effectiveness even after three days (**Figure 7A and 7B**) following sample preparation of human semen residues on fabric.

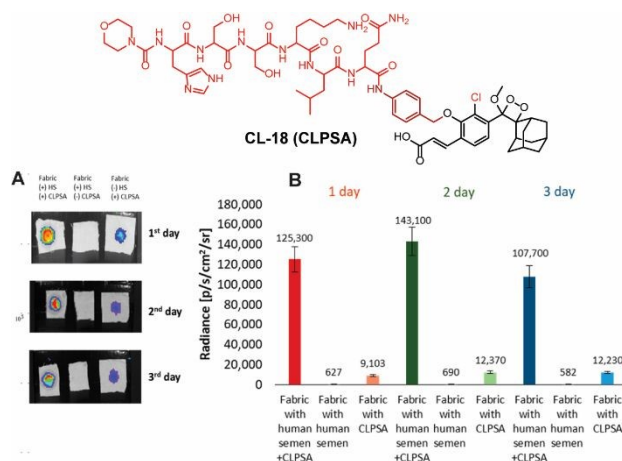


Figure 7: (A) Chemiluminescence images of human semen incubated with **CL-18** at different time intervals. (B) Chemiluminescence emission intensity quantification of Figure A. Reprinted with permission.⁸⁷ Copyright 2020 American Chemical Society.

Cathepsin B: It is a lysosomal cysteine protease (EC 3.4.22.1) responsible for protein degradation, antigen processing, and tissue remodeling.^{88, 89} It is a dipeptidyl carboxypeptidase that removes two amino acid residues from the C-terminus of a peptide substrate. The occluding loop of the active pocket contains two histidine residues located at positions 110 and 111. These histidine residues act on the C-terminal carboxylate of the substrate, thereby aiding in the facilitation of the enzyme's exopeptidase activity.⁹⁰ Within lysosomes, cathepsins are involved in the digestion of proteins and peptides, breaking them down into amino acids that can be reused for building new proteins or generating energy. It is linked to various health issues such as neck, cervical, colon, breast, and ovarian cancers, as well as neurodegenerative diseases and inflammatory disorders. This makes it a promising target for therapeutics.⁹¹⁻⁹³ To trace its activity, Shabat and coworkers chose valine-Cit dipeptide as a substrate for cathepsin B.⁹⁴ **CL-19** is comprised of conventional phenoxy-1,2-dioxetane scaffold bearing cathepsin B sensitive moiety, while **CL-20** was additionally decorated with acrylic ester to enhance the chemiluminescence efficiency. The **CL-20** was further modified with 17-mer polyethylene glycol (PEG) and KRKGC peptide to improve the aqueous solubility and cell permeability (**CL-21** and **CL-22**). PEG is well known for its hydrophilic nature and has been extensively explored for drug delivery applications.⁹⁵ The peptide (KRKGC) comprises three positively charged residues, which enhance its solubility in an aqueous system and improve the cell membrane permeability.⁹⁶ With such modifications, **CL-21** showed better chemiluminescence response than **CL-19** and **CL-20**, while **CL-22** had even more than **CL-21**. The superior chemiluminescence efficiency is attributed to the hydrophilic nature of these probes. Remarkably, **CL-22** showed a limit of detection 76.29 U/mL, which was 16000-fold superior to its fluorescent analog. Due to the large expression of cathepsin B, RAW 264.7 and CT26 cells, except for 3T3 (control group), showed bright chemiluminescence upon treatment with **CL-22**.⁹⁷ Further, to achieve NIR emission, 12-(3,5,5-trimethylcyclohex-2-en-1-ylidene)malononitrile conjugated at *para* position of phenoxy-1,2-dioxetane (**CL-23**) and dipeptide “phenylalanine-lysine” employed as a trigger for cathepsin B.⁶³ The conjugation of an extended π system at the *para* position increased the chemiluminescence quantum yield along with emission wavelength. The catalytic action of cathepsin B leads to 75.5-fold chemiluminescence enhancement at 650 nm within 30 minutes of incubation (**Figure 8A**). For *in-vivo* applications, the probe solution was injected intraperitoneally into 4T1-bearing tumor mouse models. The chemiluminescence emission attained maxima within 10 minutes of injection and it was 4-fold higher than the mouse pre-treated with cathepsin B inhibitor.

Laparotomy was conducted 30 minutes after a probe injection to illustrate the potential for precise tumor resection guided by chemiluminescence diagnosing deeply buried tumors (Figure 8B). The fluorescence signal remained undetectable in the intestinal region compared to the chemiluminescence signal. The higher signal-to-background ratio (S/B 7.6) was reported for image-guided surgery in cathepsin B expressive tissues.

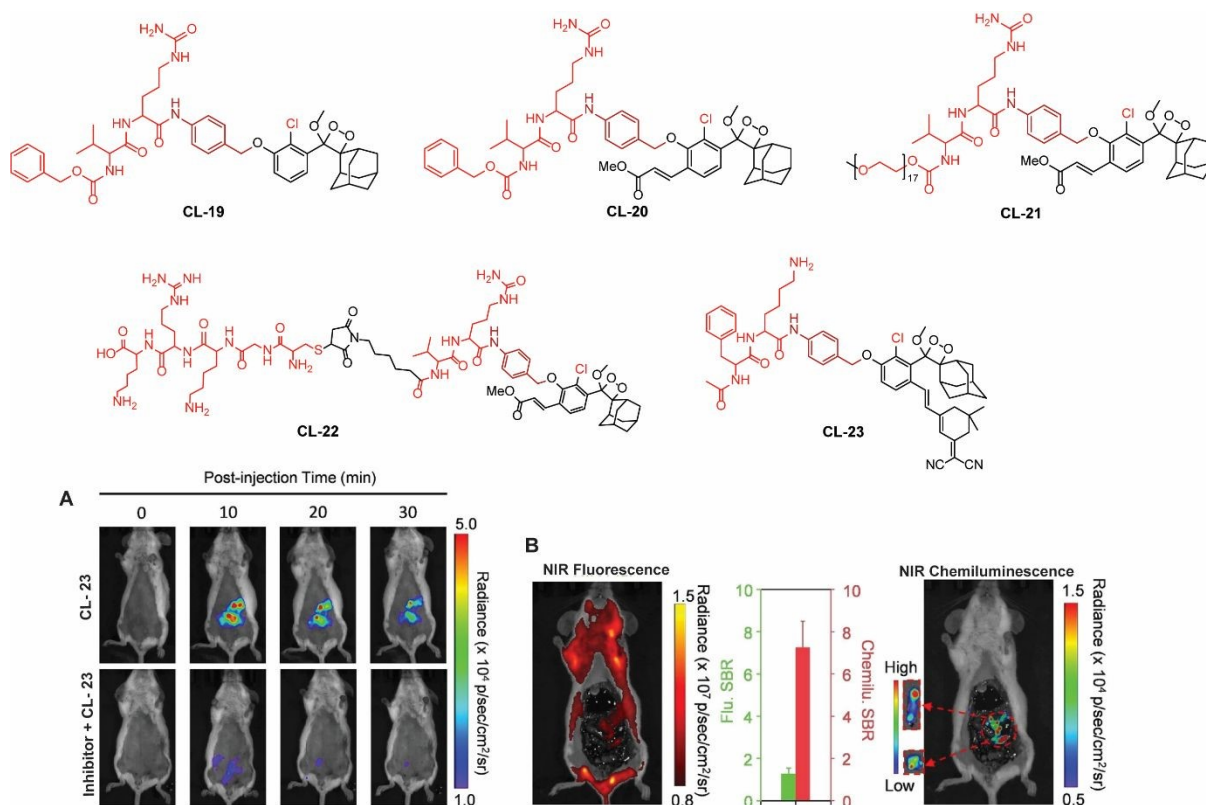


Figure 8: Chemical structure of probe CL-19 to CL-23. (A) Images of mice acquired at different time intervals after intraperitoneal injection of CL-23 (B) Fluorescence and chemiluminescence images of the intestine after laparotomy. A and B were reprinted with permission.⁶³ Copyright 2022 Wiley-VCH GmbH.

Galactosidase: Beta-galactosidase (β -Gal, EC.3.2.1.23) is a hydrolytic enzyme found in cell lysosomes that catalyses the breakdown of glycosidic linkage of oligosaccharides.⁹⁸ It is generally synthesised as 88-kDa precursor protein followed by transferring to the lysosome where it is further processed to 64-kDa active protein.^{99, 100} The detection of β -Gal levels in the human body is a critical biomarker for diagnosing primary ovarian cancer and renal disease.^{101, 102} Elevated β -Gal activity can lead to the cleavage of the glycosidic bond within the amino polysaccharide side chain and ultimately causes the breakdown of macromolecular proteoglycans and thus facilitates cancer metastasis.¹⁰³ Consequently, the development of β -Gal activatable probes holds significant importance, not only for assessing its activity but also

Open Access Article. Published on 11/12/2024. Downloaded on 11/12/2024 09:19:20. This article is licensed under a Creative Commons Attribution-NonCommercial 3.0 Unported Licence.



1
2
3 for disease diagnosis. Numerous initiatives have been undertaken to monitor the increased activity of β -Gal in various preclinical cancer models. Due to the distinctive specificity for β -galactosyl bonds, it is possible to tailor the chemiluminescence of phenoxy-1,2-dioxetane for β -Gal detection. A common approach involves the functionalisation of phenolic OH with β -galactose as a protective group. β -Gal cleaves the β -galactose on addition of substrate and thus triggers chemiluminescence.

This approach has been used by various research groups to develop numerous chemiluminescence probes. Initially, the chemiluminescence signals from Schaap's dioxetanes were enhanced through a process where energy from the excited state of the chemiluminophore was transferred to a nearby fluorophore.^{104, 105} This energy transfer led to increased light emission, serving as an indirect method to amplify chemiluminescence signals. Following similar approach, Shabat and coworkers designed and synthesised NIR Schaap's dioxetane-fluorophore conjugates (**CL-24**, **CL-25**, and **CL-26**) for detecting β -galactosidase (β -Gal) through covalent attachment of fluorophores.¹⁰⁶ Surprisingly, these probes suffered from light-induced photo decomposition except **CL-24**, which is basic Schaap's-dioxetane derivative without tethering dye. **CL-25**, linked to fluorescein, was particularly unstable under light exposure ($T_{1/2} = 45$ minutes), compared to the more stable **CL-26** ($T_{1/2} = 6$ hours). Upon β -Gal activation, **CL-26's** emission spectrum closely matched its fluorescence spectrum, confirming energy transfer from phenoxy-dioxetane to the fluorophore. **CL-26** produced a 25-fold chemiluminescence increase at 714 nm after β -Gal activation, while **CL-25** exhibited a 100-fold increase at 535 nm compared to **CL-24**. Furthermore, **CL-25** and **CL-26** were administered intraperitoneally into mice, with and without *ex vivo* exposure to β -Gal. Strikingly, **CL-26** generated a robust *in-vivo* chemiluminescence image, whereas **CL-25** remained inactive without any chemiluminescence signal (**Figure 9**). These results highlight the *in-vivo* imaging superiority of the NIR emitting **CL-26** compared to the short wavelength emitting **CL-25** probe.



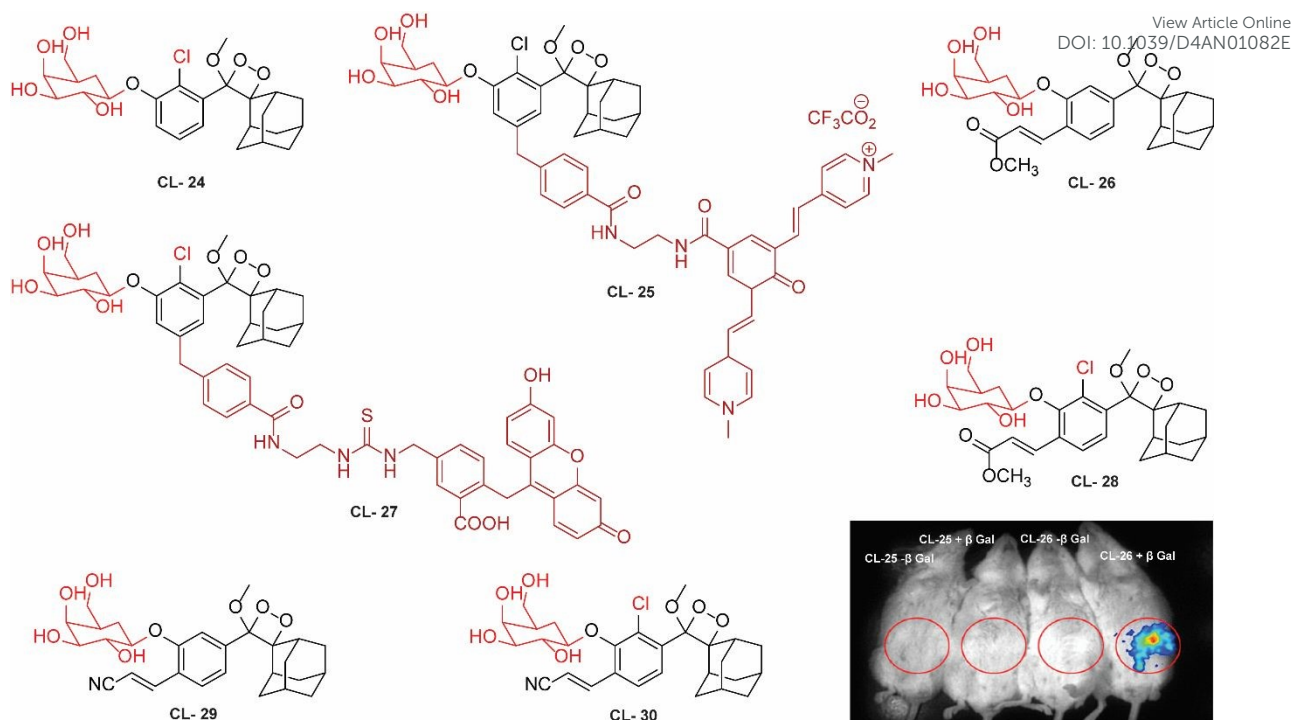


Figure 9: Molecular structure of CL-24 to CL-30. Whole body images after 15 minutes of intraperitoneal injection of CL-25 and CL-26. (Probe solution incubated with β -Gal for 30 minutes prior to injection). Reprinted with permission.¹⁰⁶ Copyright 2016 American Chemical Society

Probes using energy transfer mechanisms are structurally composed of two components: 1,2-dioxetane moiety and a fluorescent dye. This combination increases overall dimensions of the probe, which in turn limits its ability to access the active pockets of the enzyme. In contrast, a probe which consists of a smaller molecular structural framework enhances the binding interactions at the enzyme's catalytic site. Additionally, direct emitting probes exhibit superior photostability, and their chemical synthesis is comparatively straightforward. By exploring the structure-activity relationship, Shabat and coworkers modified benzoate species with different electron-withdrawing groups (EWGs) to modulate the chemiluminescent efficiency and aqueous solubility of phenoxy-dioxetane probes.⁵⁹ They addressed the steric hindrance from ortho substituents by incorporating a self-immolative linker between the phenolic oxygen and the β -Gal substrate (probes CL-27, CL-28, CL-29, and CL-30). In the presence of β -Gal, CL-27 showed a 500-fold stronger emission signal than CL-24 in an aqueous media. Interestingly, CL-28 had similar emission amplification but with an improved kinetic profile, highlighting the role of the chlorine group in chemiexcitation. When the acrylic ester group was replaced with acrylonitrile (CL-30), 1800-fold higher chemiluminescence was observed compared to CL-24. The detection limit and kinetic parameters for these probes were not reported.

For further improvements in photophysical properties, the same group has made significant advancements in developing NIR chemiluminescence turn-on probes by integrating an acceptor substituent with extended π -electron systems.⁶¹ This integration allows increased emission efficiency, resulting in more sensitive and effective probes for biological imaging and detection applications. Probe, **CL-31** was designed explicitly for β -Gal and exhibited a characteristic chemiluminescence kinetic profile with a 17-fold signal-to-noise ratio at 660 nm. The chemiluminescence intensity of transfected cells treated with **CL-31** was approximately 14 times higher than that of wild-type cells (**Figure 10A**). Furthermore, Pu and coworkers developed a NIR emitting luminescence probe (**CL-32**) by conjugating dicyanomethylene-4H-benzothiopyran with phenoxy-1,2-dioxetane moiety.⁶² It showed 85.6-fold chemiluminescence enhancement when treated with β -Gal, with a detection limit of 73 mU/L. SKOV3 cells exhibited a 13-fold increase in emission compared to HeLa cells within 30 minutes of treatment. In SKOV3 tumor-bearing mice, the chemiluminescence signal increased progressively after intratumoral injection, and at 20 minutes, SKOV3 tumors displayed a 6.5-fold higher signal compared to HeLa tumors (**Figure 10B**). Despite these promising results, an accurate delivery of such probes into cancer cells is very challenging issue. Numerous strategies have been adopted to improve the cell specificity including anchoring of cell surface receptor-specific moiety to cellular tracker.^{107, 108} In this direction, Shabat and coworkers anchored tumor cell-specific peptide "CGKRRK" to probe *via* a maleimide-based linker.¹⁰⁹ This approach not only improved the aqueous solubility but also directed probe to tumor cells.¹⁰⁹ The effectiveness of two probes, **CL-33a** and **CL-33b**, in imaging β -Gal activity was tested in mice with CT26 tumors. Direct injection of these probes into tumor sites showed that CT26-LacZ tumors injected with **CL-33b** exhibited a chemiluminescence signal approximately 20 times stronger than CT26-WT tumors, while **CL-33a** remained inactive (**Figure 10C**). This significant enhancement in chemiluminescence was attributed to the lower pKa of the phenoxy-1,2-dioxetane bearing a chlorine substituent, which promoted chemiexcitation in the mildly acidic tumor microenvironment.

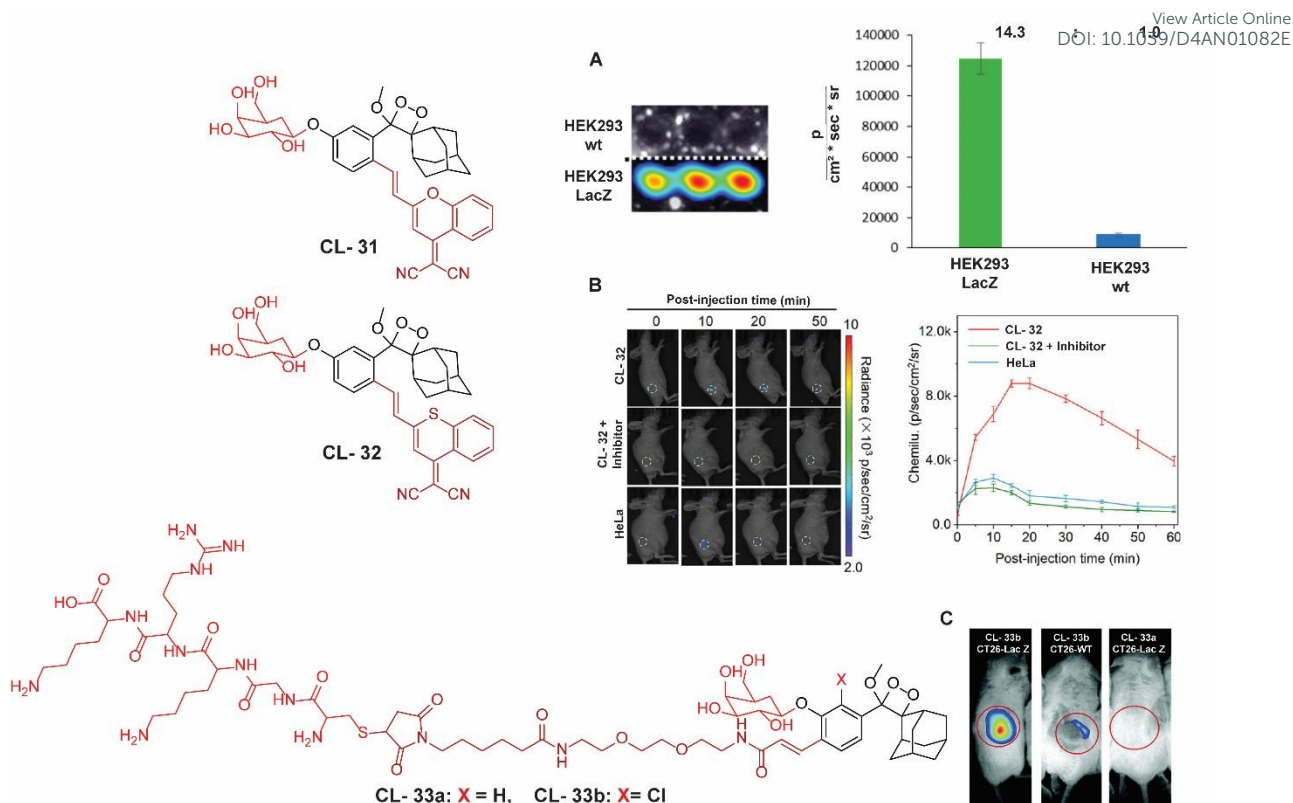


Figure 10: Molecular structure of **CL-31** to **CL-33**. (A) Imaging of cell line upon treatment with **CL-31** and quantification of emission intensity. Figure reproduced with permission.⁶¹ Copyright © 2017, American Chemical Society (B) *In-vivo* imaging of tumor-bearing mice upon treatment with **CL-32**. Reproduced with permission.⁶² Copyright© 2020 Wiley-VCH GmbH (C) *In-vivo* imaging of tumor-bearing mice upon treatment with **CL-33b** Reproduced with permission.¹⁰⁹ Copyright © 2018 Royal Society of Chemistry.

Monitoring low drug concentrations in individual patients is a challenge, impeding clinicians' ability to personalise treatments.¹¹⁰⁻¹¹² As a result, there's an apparent necessity for novel cancer therapies that not only minimise side effects but also enable real-time imaging of drug bio-distribution. One promising approach is to analyse drug release through chemiluminescence, which offers a superior signal-to-noise ratio in living tissues. Doron and coworkers devised a theranostic prodrug, **CL-34** to deliver monomethyl auristatin E in response to β -Gal activity.¹¹³ The activation of prodrug by β -Gal was accompanied by direct emission of green light, with a linear correlation between light emission at 555 nm and the release of free drug. The activation of the prodrug with chemiluminescence enhancement is shown in **Figure 11A**. In HEK293-LacZ cells, treatment with the prodrug led to a 25-fold increase in chemiluminescence compared to wild-type HEK293 cells (Figure 11B), and the IC₅₀ was reduced by a factor of 20 in HEK293-LacZ cells. Increased chemiluminescence in HEK293-LacZ versus wild type of HEK293 revealed higher β -Gal expression. Additionally, mice bearing CT26-LacZ tumors



treated with CL-34 showed approximately five times higher chemiluminescence compared to those treated with the control prodrug (**Figure 11C**).

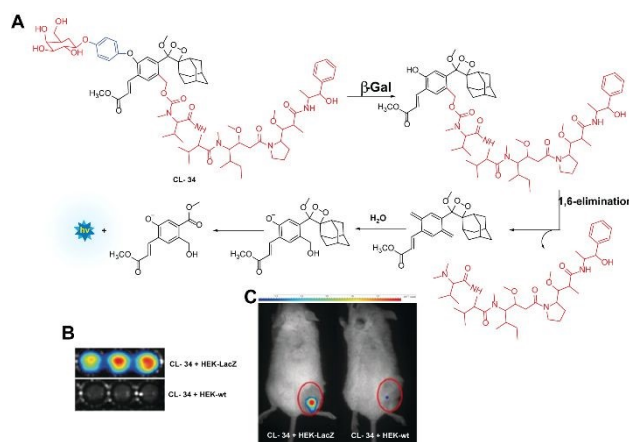
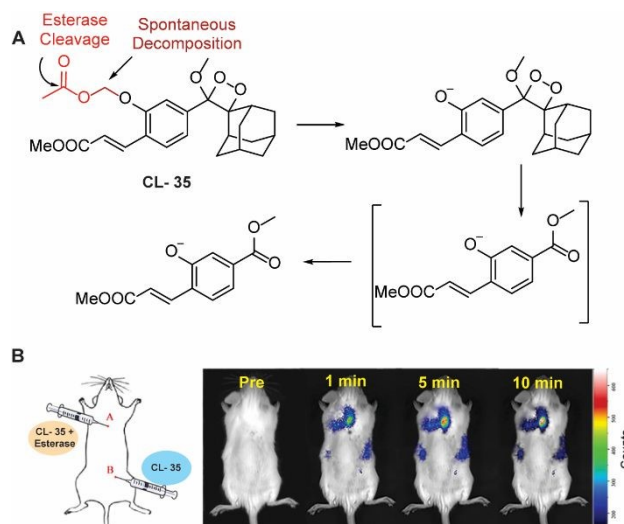


Figure 11: (A) Molecular mechanism of drug releases from CL-34 in the presence of β -Gal. (B) Chemiluminescence images of mammalian cells upon treatment with prodrug. (C) Whole-body imaging of mice upon treatment with prodrug CL-34.¹¹³ Copyright © 2018 Wiley-VCH Verlag GmbH & Co. KGaA, Weinheim.

Esterases (EC 3.1) are classified under the hydrolase class, capable of hydrolysis of esters into alcohols and acids. A wide range of enzymes, including acetylcholinesterase, carboxylesterase, lipase, etc. are classified under the hydrolase enzyme class.^{114, 115} They perform critical operations in biological systems such as ester metabolism, substance transportation, and gene expression. Their absence or abnormal expression leads to the pathogenesis of Wolman disease, cancer, and hyperlipidemia.¹¹⁶ As a result, the development of novel and efficient esterase assays has considerable importance for the diagnosis and staging of numerous ailments. Recently, to monitor its activity, Chen and coworkers masked phenolic OH of phenoxy-1,2-dioxetane with acetoxymethyl ether (**CL-35**). Hydrolysis of ester bond in the presence of esterase was followed by release of phenoxy-1,2-dioxetane through a 1,6-elimination rearrangement reaction as shown in **Figure 12A**. the probe's emission reached saturation at 540 nm within 20 minutes, with a detection limit calculated at 1.90×10^{-3} U/mL.¹¹⁷ Chemiluminescence intensity showed a linear relation with varying esterase concentrations. Additionally, a time-dependent change in emission was observed at the injection site when the probe solution, with or without esterase, was injected subcutaneously into animal models (**Figure 12B**).





View Article Online
DOI: 10.1039/D4AN01082E

Figure 12: (A) Activation mechanism of CL-35 in the presence of esterase. (B) Chemiluminescence monitoring in animal models. Reprinted with permission.¹¹⁷ Copyright © 2022 Elsevier B.V.

3.2 Oxido-Reductase

Nitroreductase (NTR): NTR is a flavin-containing redox enzyme that participates in the reduction of nitro-containing compounds in organisms.¹¹⁸ Under hypoxic conditions, it facilitates the electron transfer reduction of nitro groups to hydroxylamines, subsequently converting it into amines in the presence of nicotinamide adenine dinucleotide (NADH).¹¹⁹ Based on their catalytic activity, NTRs were categorised into two types: type I, which are oxygen-insensitive, and type II, which are oxygen-sensitive.¹²⁰ Type II NTRs facilitate the one-electron transfer reduction of nitro groups, producing superoxide anions. Type I NTRs are further subdivided into major and minor groups based on their cofactor preferences. These class of enzymes function as homodimers with flavin mononucleotide (FMN)-binding sites necessary for their activity. They operate through a ping-pong bi-bi redox mechanism, utilising a nicotinamide cofactor to transfer electrons and reduce nitroaromatic compounds.^{121, 122} Due to their close association with hypoxic environments in living cells, NTRs have been extensively studied for imaging of cancer cells and drug delivery applications. In tumor microenvironment, hypoxia often leads to increased levels of NTR; however, it is scarcely expressed in normal tissues.^{123, 124} Numerous NTR-responsive chemiluminescent probes and drug delivery systems have been developed, and extensively utilised for cellular imaging.^{125,}

126

Lippert and coworkers utilised *para*-nitrobenzyl moiety as a triggering substrates (CL-36 and CL-37) for imaging of NTR.⁴² The *para*-nitrobenzyl group underwent self-immolative

cleavage when exposed to an enzyme in the presence of NADH. This process led to liberation of phenolate-1,2-dioxetane which subsequently undergo the CIEEL mechanism and emits light. Furthermore, the chemiluminescence emission improved with the addition of 10% Emerald II. Emerald II is an aqueous solution that contains a polymer imparts hydrophobic environment to the chemiluminophore and thus diminishes the quenching effect of water molecules. Probe, **CL-37** showed a significantly improved signal-to-noise ratio (172-fold) and selectivity over biothiols compared to **CL-36**. The limit of detection calculated for **CL-37** was 1.9 ng/mL. In experiments with tumor xenograft SCID/BALB-C mice, hypoxic conditions were maintained in environments with 21% and 100% oxygen. Notably, the animal exposed to oxygen-deficient conditions exhibited brighter chemiluminescence than those in oxygen-rich environments (**Figure 13A**). However, the authors found that use of cationic polymer caused toxicity to living tissues and thus limited their clinical applicability.¹²⁷ To address this issue, Zhang and coworkers synthesised a water-soluble probe (**CL-38**) by introducing electron withdrawing carboxylate substituent *ortho* to NTR trigger.¹²⁸ This probe showed 6000-fold chemiluminescence enhancement upon incubation with NTR/NADH even without an additional enhancer and had a detection limit of 0.947 ng/mL, significantly surpassing **CL-36**. Further, probe solution was injected intratumorally to visualise the degree of hypoxia in A459 tumor-bearing mice models. **CL-38**'s chemiluminescence correlated directly with the tumor's hypoxic state (**Figure 13B**), revealing a mean photon flux intensity in hypoxic mice 4.5 times greater than in those with sufficient oxygen. While probes, **CL-37** and **CL-38** responded to tissue oxygenation in animal models, however, their cell lines studies were not explored. To fill this gap, Lippert and coworkers reported the effectiveness of **CL-39** and **CL-40** chemiluminescent reporters for hypoxia across various settings: *in-vitro*, within cellular environments, and *in-vivo*.¹²⁹ **CL-40** showed 37-fold chemiluminescence enhancement in 80 minutes in rat liver microsomes, while **CL-39** exhibited an extraordinary 60,000-fold enhancement in just 20 minutes. The drastic increase in chemiluminescence response and ultra-sensitivity of **CL-39** was attributed to acetoxymethyl ester, which improved its cellular uptake. Additionally, **CL-40** was successfully utilised to discriminate between hypoxic and normoxic conditions in A549 cells, images taken 60 minutes post-injection revealing distinct contrasts between hypoxic and well-oxygenated tissues (**Figure 13C**). The photon flux intensity (1×10^7 photons/s) of **CL-39** was 100 times greater than that of **CL-37** and CL-NTR. These findings suggest that positioning of EWG substituents at the *para* position of phenolic OH is a critical component to improve the chemiluminescence emission and sensitivity. Moreover, integrating

hydrophobic groups, such as esters, alongside EWGs could further facilitate cellular uptake. Future structural modifications may enhance the photophysical properties and cellular uptake of phenoxy-1,2-dioxetane derivatives.

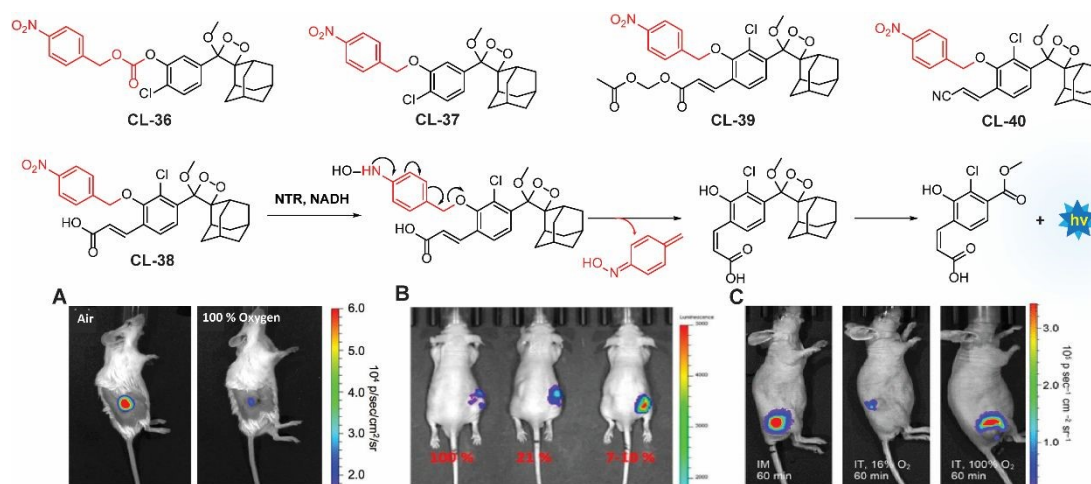


Figure 13: Molecular structure of **CL-36** to **CL-40**. (A) Images of living H1299 lung tumor bearing mice 1.5 min after administering intratumoral injections **CL-37** and 10% Emerald II Enhancer. Figure reproduced with permission.⁴² Copyright © 2016 American Chemical Society (B) Images of tumor (A549) within 10 minutes of Intratumoral injection of **CL-38**. Reproduced with permission.¹²⁸ Copyright © 2018 American Chemical Society (C) Images of animal models bearing tumor after injection with **CL-40**. Figure Reproduced with permission.¹²⁹ Copyright © 2019 American Chemical Society.

NAD(P)H Quinone Oxidoreductase 1 (DT-diaphorase; EC 1.6.5.2): It is an intracellular flavoenzyme, that regulates the redox state by facilitating the two-electron reduction reaction of quinones to their respective hydroquinones.¹³⁰ It works almost with similar efficiency in the presence of cofactors NADPH or NADH. It is a homodimer having two active pockets where the FAD cofactor is bound tightly.¹³¹ Its significant overexpression (5–200 fold) in numerous types of tumors makes it responsible for multiple carcinogenic processes. This heightened expression in tumors highlights the necessity for developing sensitive probes that can detect cancer subtypes associated with high NQO1 levels.¹³² To track NQO1 activity in both *in-vitro* and *in-vivo* models, chemiluminophores are generally conjugated with a quinone-based substrates that undergo bio-reduction. Kim and coworkers investigated chemiluminescence of phenoxy-1,2-dioxetane by covalently tethering it with trimethyl-locked quinone through a self-immolative linker (**CL-41**).¹³³ This probe, when bio-catalysed by NQO-1, showed 130-fold chemiluminescence enhancement at 515 nm, with a detection limit of 51 ng/mL. The quinone reduction mechanism followed by light emission is shown in **Figure 14A**. Additionally, A549 cells showed 34 times more chemiluminescence than H596 cells when treated with **CL-41**. NQO1 activity was also visualised in A549 and H596-derived xenografts, where A549 tumor-



bearing mice showed strong bright chemiluminescence while no apparent signal was obtained in H596 ones (**Figure 14B**). Shabat and coworkers extended this work by synthesising acrylonitrile (**CL-42**) and styryl-substituted probes (**CL-43**) to detect varying concentrations of NADH in the presence of NQO1. **CL-42** showed rapid chemiexcitation than **CL-41**, with a limit of detection of 8 nM, while **CL-43** exhibited 4-fold higher sensitivity, achieving a detection limit of 2 nM. This improvement is attributed to the styryl group, which enhances the reactivity of phenolate anions. Later, the same group designed the probe **CL-44** to improve the emission wavelength and aqueous solubility.⁴³ It showed remarkable 310-fold emission enhancement at 610 nm in response to NQO-1. However, mammalian cell line studies were not conducted with this probe.

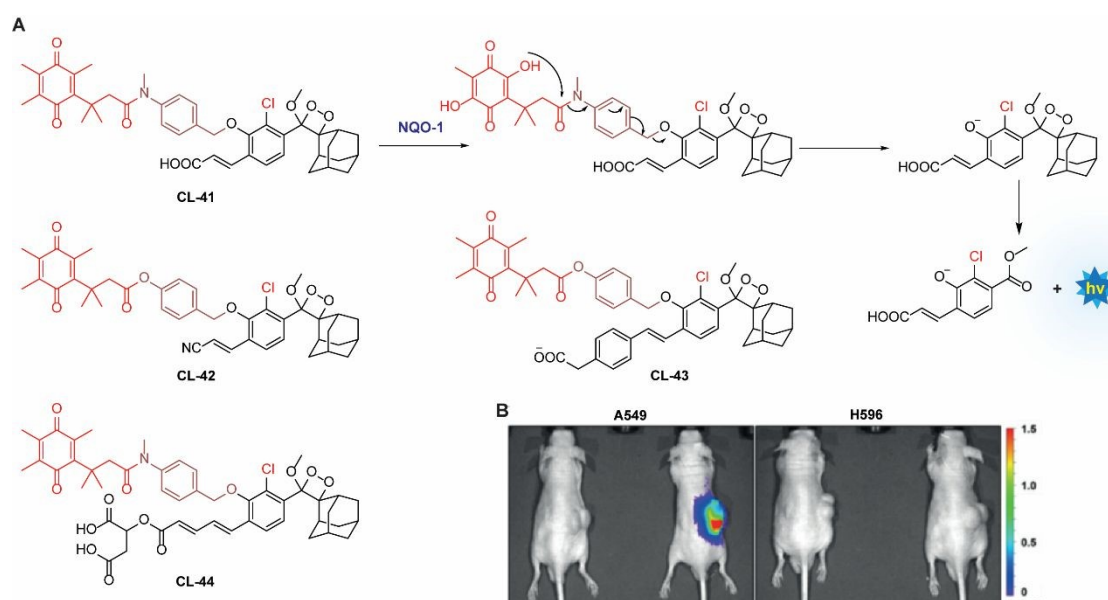


Figure 14: (A) Activation mechanism of CL-41 in the presence of NQO-1. (B) *In-vivo* imaging of NQO-1 upon treatment with CL-41. Reprinted with permission.¹³³ Copyright © 2019 Wiley-VCH Verlag GmbH & Co. KGaA, Weinheim.

Lysyl oxidase (LOX): It is a protein-lysine 6-oxidase (EC 1.4.3.13), which catalyses the deamination reaction of amino acids to promote crosslinking in collagen and elastin tissues, thereby enhancing the structural integrity of the ECM proteins.^{134, 135} The enzyme's catalytic site contains copper-binding domains, which are essential for its activity. It is an ECM protein secreted by tumor cells to foster tumor growth and metastasis.^{136, 137} Consequently, LOX has garnered significant attention as a potential therapeutic target in cancer treatment, and efforts are underway to develop a synthetic chemiluminescent reporter for monitoring LOX activity. Pu and coworkers developed activatable chemiluminescent probes for targeted photodynamic cancer therapy (PDT).¹³⁸ They modified the malonitrile group of dicyanomethylene-4H-

Open Access Article. Published on 18/11/2024. Downloaded on 18/11/2024 09:14:20. This article is licensed under a Creative Commons Attribution-NonCommercial 3.0 Unported Licence.



benzopyran-phenoxy-dioxetane by replacing it with benzoylacetonitrile, 1,3-dimethylbarbituric acid, and 1,3-diethyl-2-thiobarbituric acid to narrow the energy gap. Three different probes (**CL-45a**, **CL-45b**, **CL-45c**) have been developed and further modified to track LOX activity. These probes exhibited redshifted chemiluminescence emissions to 700, 738, and 742 nm with half-lives of 178, 62, and 114 minutes, respectively. Based on the highest single oxygen-generating capacity of **CL-45b** for PDT, its chemiluminescence was masked with propylamine to target LOX (**CL-46**). Upon activation by LOX within 30 minutes, **CL-46** showed a remarkable 19.1-fold enhancement in chemiluminescence, with a limit of detection of 0.013 U/mL. Mice bearing 4T1 tumors were injected with a probe intratumorally followed by immediate chemiluminescence imaging for 80 minutes, achieving peak brightness in just 3 minutes (**Figure 15**). The tumor-to-background ratio was reported to be 14.6, which was 3.04 times higher than that observed in the β -aminopropionitrile (LOX inhibitor) group. Subsequently, light irradiation for PDT resulted in complete inhibition of tumor growth.

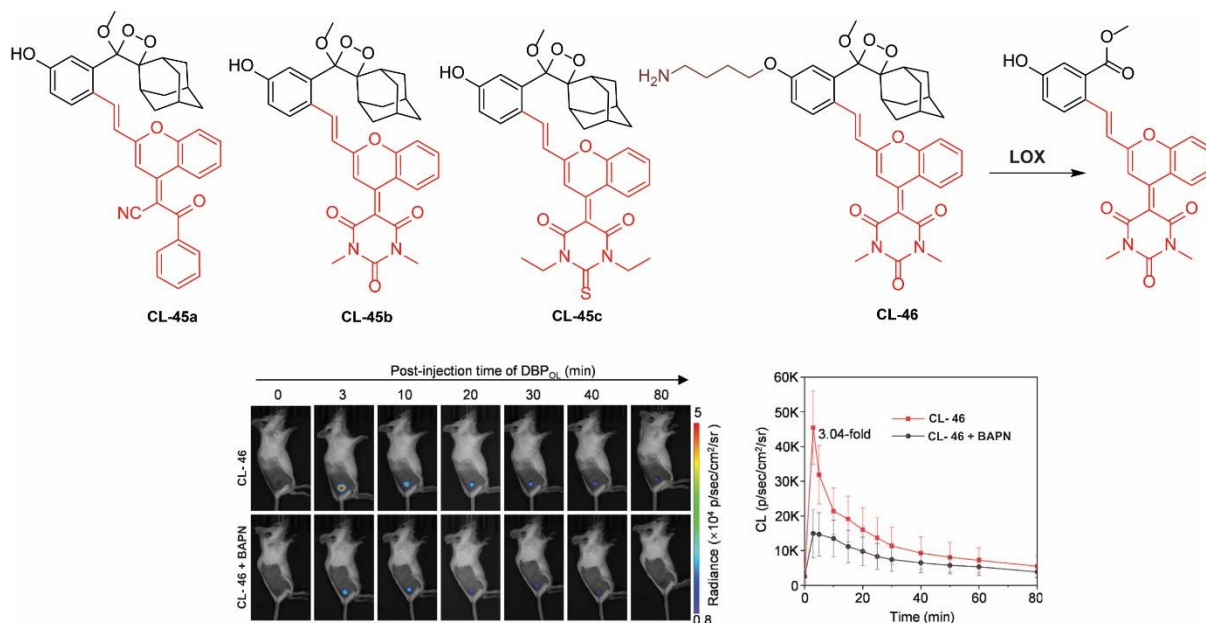


Figure 15: Molecular structure of CL-45 to CL-46. Chemiluminescence images of animal models upon treatment with CL-46 and quantification of emission intensity.¹³⁸ Copyright © 2023 Wiley-VCH GmbH.

Tyrosinase: It is a copper-containing metalloenzyme (EC 1.14.18.1) involves in the synthesis of melanin pigment in the skin.¹³⁹ It catalyses the *ortho*-hydroxylation of monophenol to diphenol, followed by the formation of corresponding quinone, and leads to an unusual accumulation of melanin in skin cells.¹⁴⁰ Due to its ability to oxidise small phenolic molecules, the chemiluminophores are modified with triggering units containing *para*- or *meta*-phenol groups. Based on the enzyme-substrate reaction mechanism, Sessler and coworkers developed

Open Access Article. Published on 18/11/2024. Downloaded on 18/11/2024 09:14:20. This article is licensed under a Creative Commons Attribution-NonCommercial 3.0 Unported Licence.



tyrosine-based chemiluminescent probes (**CL-47**, **CL-48**, and **CL-49**).¹⁴¹ In this system, tyrosinase-mediated catalysis leads to the formation of stable *ortho*-benzoquinone intermediates, resulting in a poor chemiluminescence response. However, when thiols are introduced, they fully reduce the intermediate through 1,6-elimination, releasing benzoate intermediates and resulting in robust chemiluminescence (**Figure 16**). The addition of thiols to the reaction solution improved the chemiexcitation by 430-fold compared to the response with tyrosinase alone. Thiol conjugation to benzoquinone promoted the 1,6-elimination reaction and resulted in enhanced chemiexcitation. For **CL-47**, the detection limit was determined to be 0.1 U/mL with varying enzyme concentrations in the presence of glutathione. The inferior response of **CL-48** compared to **CL-47** is attributed to its sterically hindered structure. Additionally, the presence of a carboxylic group limited cell permeability, leading to further modification of **CL-47** by adding a 2-dimethylaminoethyl group to create **CL-49**. Notably, **CL-49** exhibited a 2.6-fold higher chemiluminescent response in B16 cells compared to EMT6 cells, indicating its ability to differentiate between cell lines. However, the inherent limitation of the 'AND' logic operation lies in the inability to monitor tyrosinase activity independently without adding thiols. This highlights significant demand for a system capable of monitoring two species through independent emission channels.

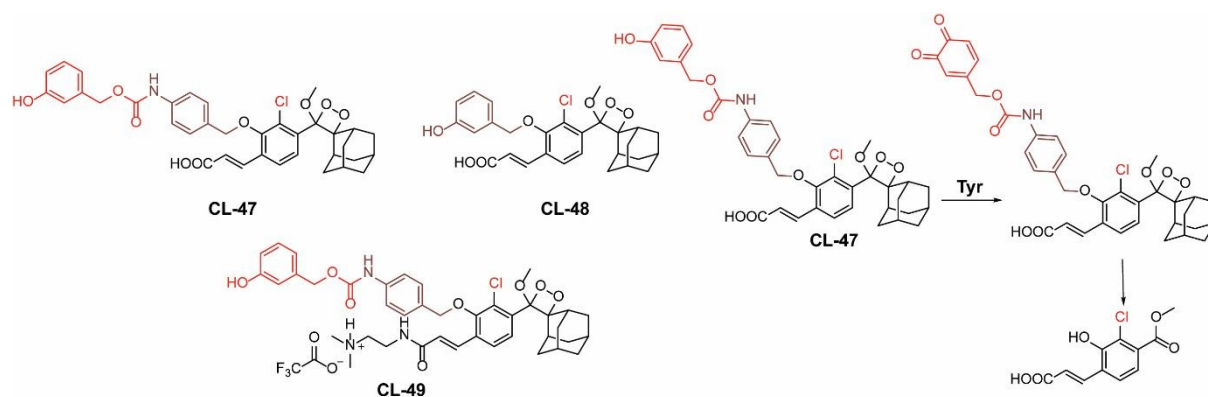


Figure 16: Molecular structure of **CL-47-49** and reaction mechanism outline for tyrosinase detection.

3.3 Transferase

Gamma-glutamyl transpeptidase (EC 2.3.2.2) is a cell membrane-bound transferase enzyme crucial for maintaining glutathione and cysteine homeostasis by breaking down γ -glutamate in glutathione.^{142, 143} Abnormal activity of this enzyme is associated with liver dysfunctions, asthma, diabetes, and the pathogenesis of cancer.¹⁴⁴ Therefore, researchers are tracing its activity noninvasively in living cells and animal models to identify the diseased cells. Ye and



coworkers employed modified Schaap's dioxetane substituted with acrylic ester to track the activity of glutamyl transpeptidase (CL-50).¹⁴⁵ Similar to previous probes, this probe incorporates a phenoxy-1,2-dioxetane structure anchored with the recognition unit γ -glutamic acid, facilitating interaction with the enzyme's active site (**Figure 17A**). It showed a significant 876-fold increase in chemiluminescence within 30 minutes of incubation with glutamyl transpeptidase. The chemiluminescence peaked in intensity within 15 minutes and remained detectable for over 45 minutes in OVCAR5 and U87MG cells. In these cancer cells, the average chemiluminescence intensity was approximately 29-fold and 23-fold higher, respectively, compared to HUVEC cells. In tumor-bearing mice, intravenous administration showed a gradual increase in the chemiluminescence till 12 minutes before returning close to background levels after 1 hour (**Figure 17B**). Inhibition of glutamyl transpeptidase activity with GGsTop in U87MG tumors suppressed the chemiluminescence during imaging. Quantitative analysis revealed that the intensity of chemiluminescence in cancerous cells treated with CL-50 was 2.1 times greater than in tumors treated with GGsTop. A summary of the phenoxy-1,2-dioxetane is provided in Table 3.

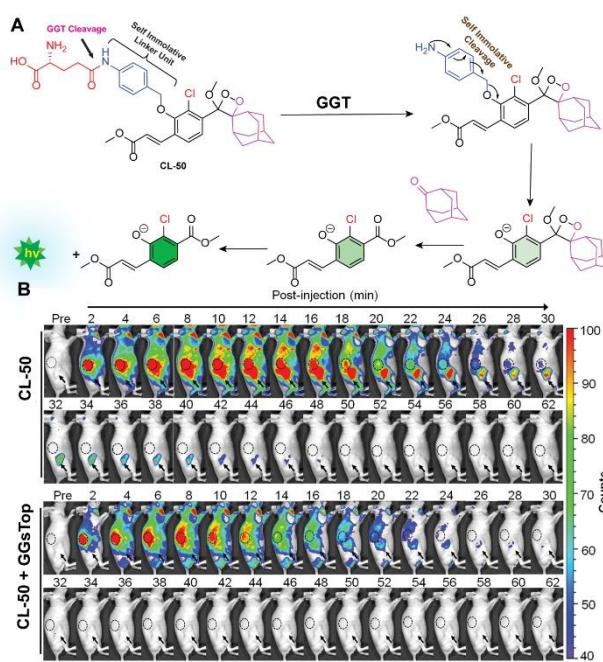


Figure 17: (A) Activation mechanism of CL-50 upon incubation with glutamyl transpeptidase. (B) Real-time chemiluminescence images of U87MG-tumor-bearing mice after injection of CL-50. Reprinted with permission.¹⁴⁵ Copyright © 2019 American Chemical Society

Table 3: Summary of Phenoxy-1,2-dioxetane Derivatives Discussed in this Review



Pro be	Enzyme	LOD	Mice/Injection	Fold Enhance ment	λ_{em} (nm)	Cell Type	ϕ (Ein stein /mol)	$T_{1/2}$	Refer ence
CL-12a	FAP α	0.785 ng/mL	6-week-old male BALB/c nude mice, IT	121	-	HepG2	-	-	70
CL-12c	FAP α	0.965 ng/mL	-	-	-	HepG2	-	-	
CL-12c	FAP α	0.587 ng/mL	-	-	-	HepG2	-	-	
CL-13	Granzyme B	0.7 nM	NSG mice, IT	139	520	NK cells	-	-	71
CL-14	Aminopeptidase N	0.53 ng/mL	nude BALB/c mice	26	510	HepG2	-	-	79
CL-15	Aminopeptidase N	0.056 ng/ml	3-5-week-old BALB/c nude mice	-	540	HepG2	-	-	80
CL-16	Aminopeptidase N	0.068 U/mL	6-week-old BALB/c nude mice, IT	53	560	HepG2 and LO2	-	-	81
CL-17a	LAP	0.008 U/mL	4-5-week-old BALB/c nude mice, IT	1260	550	HepG2 and LO2	-	-	83
CL-17b	LAP	Inactive	-	-	-	-	-	-	
CL-18	PSA	-	-	157			-	-	87
CL-22	Cathepsin B	76.29 mU/mL	-	-	540	RAW 246.7, CT26, and 3T3	-	-	97
CL-23	Cathepsin B	-	-	75.5	650	4T1	-	-	63
CL-24	β -Gal	-	-	-	-		-	-	106
CL-25	β -Gal	4.0×10^{-3} units/mL	BALB/c female mice, IP	100	535	HEK293-LacZ	3.8×10^{-3}	170 min	
CL-26	β -Gal	-	BALB/c female mice, IP	25	714	HEK293-LacZ	9.0×10^{-4}	100 minutes	
CL-31	β -Gal	-	-	17	660	HEK293-LacZ	0.82×10^{-2}	178 Minutes	61

CL-32	β -Gal	73 mU/mL	adult female Ncr nude mice, IT	85.6	760	SKOV3	0.23×10^{-2}	62	109
CL-33a	β -Gal	-	7-week-old BALB/c female mice, IT	-		CT26	-	-	109
CL-33b	β -Gal	-	7-week old BALB/c female mice, IT	30		CT26	-	-	
CL-34	β -Gal	-	BALB/c, IT	25	555	HEK293-LacZ	-	-	113
CL-35	Esterase	1.90×10^{-3} U/mL	-	-	540	HeLa	-	-	117
CL-37	NTR	1.9 ng/mL	6-week old BALB/c female mice, IT	172	545	-	-	-	42
CL-38	NTR	0.947 ng/mL	SCID/BALB-C, IT	6000	-	-	-	-	128
CL-39	NTR	-	-	60000	516	-	-	-	129
CL-40	NTR	-	athymic nude mice	37	525	A549	-	-	
CL-41	NQO-1	51 ng/mL		130	515	A549	-	-	132
CL-42	NQO-1	8 nM for NADH	-	-	-	-	-	-	60
CL-43	NQO-1	2 nM for NADH	-	-	-	-	-	-	
CL-44	NQO-1	-	-	310	610	-	-	-	43
CL-46	LOX	0.013 U/mL	BALB/c mice (female, 5 weeks old), IT	19.1	720	4T1	-	-	138
CL-47	Tyrosinase	0.1 U/ml.	-	430	540	B16	-	-	141
CL-50	γ -glutamate	16 mL/U	Female, athymic, 6–8 weeks old, BALB/c mice	876	-	U87MG	-	-	145

4 Conclusion and Perspective

This review highlights the advancements in phenoxy-1,2-dioxetanes as chemiluminophores for diagnostic applications, focusing on a multidisciplinary approach that combines expertise in organic chemistry, biochemistry, cell biology, and photophysics. Tables 1 and 2 present various design strategies for chemiluminophores aimed at enhancing photophysical properties, such as emission maxima, quantum yield, and pKa, of phenoxy-1,2-dioxetanes. Meanwhile, Table 3 provides an overview of different 1,2-dioxetane chemiluminophores, categorised based on their



selectivity for specific enzyme classes relevant to various diseases and their use in bio-imaging applications.

Despite the advances in activatable probes for bio-imaging, research on chemiluminescence-based approaches remains in its early stages. The reported chemiluminescence probes for imaging endogenous enzymes meet several obstacles including low emission intensity, emission at shorter wavelength, and shorter luminescence lifetime. Therefore, extensive investigation into structural modifications of phenoxy-1,2-dioxetanes is needed to enhance chemiexcitation, emission wavelength, and luminescence half-life. Previously, various methods have been employed to achieve near-infrared (NIR) emission for deep-tissue imaging, including the conjugation of fluorescent dyes with phenoxy-1,2-dioxetane and the addition of electron-withdrawing groups (EWGs) at the ortho and para positions of phenol. However, these approaches increase the overall size of the probe, limiting its ability to enter the enzyme's active site and often resulting in compromised quantum yield. Therefore, more structural modifications are necessary to improve the brightness. Additionally, tuning the pKa of the phenolic OH group is critically important for effective bio-imaging at physiological pH. The kinetic parameters, including the Michaelis-Menten constant and V_{max} , are crucial in determining probes' affinity for particular enzymes. However, this study is unavailable for the chemiluminescent probes discussed in this review. Evaluating parameters such as K_{cat} and the substrate's association constant with the enzyme could significantly enhance the design strategies for enzyme-specific probes.

Among the wide range of enzymes involved in cellular metabolism and disease progressions, only a few have garnered attention for the development of chemiluminescent probes. The continuous advancements in chemical biology and medicinal chemistry are expected to enhance our understanding of the precise reaction sites within enzymes and biomarkers, paving the way for the development of new chemiluminescent enzyme probes. We anticipate that these probes will emerge as indispensable tools in both diagnostics and theranostics. This review provides valuable insights for aspiring researchers entering this field.

Conflict of Interest: All the authors declare no conflict of interest

Data Availability: No primary research results, software, or code have been included and no new data were generated or analysed as part of this review.

Acknowledgment

View Article Online
DOI: 10.1039/D4AN01082E

J S Sidhu acknowledges the BITS-Pilani, Pilani campus for providing infrastructure and research facilities. MKC would like to thank the Royal Society of Chemistry (R23-0850952021) and University of Kent for funding.

References

1. M. Zhao, B. Li, H. Zhang and F. Zhang, *Chem. Sci.*, 2021, **12**, 3448-3459.
2. V. Naresh and N. Lee, *Sensors (Basel)*, 2021, **21**, 1109
3. S. He, J. Song, J. Qu and Z. Cheng, *Chem. Soc. Rev.*, 2018, **47**, 4258-4278.
4. E. A. Owens, M. Henary, G. El Fakhri and H. S. Choi, *Acc. Chem. Res.*, 2016, **49**, 1731-1740.
5. J. A. Thomas, *Chem. Soc. Rev.*, 2015, **44**, 4494-4500.
6. A. Fernández and M. Vendrell, *Chem. Soc. Rev.*, 2016, **45**, 1182-1196.
7. S. Yoon, S. Y. Cheon, S. Park, D. Lee, Y. Lee, S. Han, M. Kim and H. Koo, *Biomater Res*, 2022, **26**, 57.
8. A. Ji, H. Lou, J. Li, Y. Hao, X. Wei, Y. Wu, W. Zhao, H. Chen and Z. Cheng, *Chem. Sci.*, 2024, **15**, 3339-3348.
9. Y. Shi, Y. Hu, N. Jiang and A. K. Yetisen, *ACS Sens.*, 2022, **7**, 1615-1633.
10. W. L. Rice, D. M. Shcherbakova, V. V. Verkhusha and A. T. N. Kumar, *Cancer Res.*, 2015, **75**, 1236-1243.
11. O. Green, T. Eilon, N. Hananya, S. Gutkin, C. R. Bauer and D. Shabat, *ACS Cent. Sci.*, 2017, **3**, 349-358.
12. Y. Yang, S. Wang, L. Lu, Q. Zhang, P. Yu, Y. Fan and F. Zhang, *Angew. Chem. Int. Ed.*, 2020, **59**, 18380-18385.
13. Y. Liu, J. Tan, M. Wan, L. Zhang and X. Yao, *ACS Omega*, 2020, **5**, 15922-15930.
14. A. Lyu, Y. Wang and H. Cui, *Anal. Chem.*, 2023, **95**, 7914-7923.
15. A. Roda, M. Mirasoli, E. Michelini, M. Di Fusco, M. Zangheri, L. Cevenini, B. Roda and P. Simoni, *Biosens. Bioelectron.*, 2016, **76**, 164-179.
16. S. Emdadi, M. H. Sorouraddin and L. Denanny, *Analyst*, 2021, **146**, 1326-1333.
17. X. Lu, X. Song, Q. Wang, W. Hu, W. Shi, Y. Tang, Z. Wu, Q. Fan and W. Huang, *RSC Adv.*, 2020, **10**, 11861-11864.
18. U. Haris and A. R. Lippert, *ACS Sens.*, 2023, **8**, 3-11.
19. H. Gunduz, T. Almammodov, M. Dirak, A. Acari, B. Bozkurt and S. Kolemen, *RSC Chem. Biol.*, 2023, **4**, 675-684.
20. Y. Yang and F. Zhang, *Analysis Sensing*, 2021, **1**, 75-89.
21. A. V. Romanyuk, I. D. Grozdova, A. A. Ezhov and N. S. Melik-Nubarov, *Sci. Rep.*, 2017, **7**, 3410.
22. M. A. Tzani, D. K. Gioftsidou, M. G. Kallitsakis, N. V. Pliatsios, N. P. Kalogiouri, P. A. Angaridis, I. N. Lykakis and M. A. Terzidis, *Molecules*, 2021, **26**, 7664.
23. L. Yue and Y.-T. Liu, *J. Phys. Chem. B.*, 2020, **124**, 7682-7693.
24. H. An, C. Guo, D. Li, R. Liu, X. Xu, J. Guo, J. Ding, J. Li, W. Chen and J. Zhang, *ACS Appl. Mater. Interfaces.*, 2020, **12**, 17230-17243.
25. R. C. Allen, *Antioxidants*, 2022, **11**, 518.
26. H. Karatani, *Anal. Sci.*, 2022, **38**, 613-621.
27. J. Zhang, C. Wickizer, W. Ding, R. Van, L. Yang, B. Zhu, J. Yang, Y. Wang, Y. Wang, Y. Xu, C. Zhang, S. Shen, C. Wang, Y. Shao and C. Ran, *Proc. Natl. Acad. Sci. U. S. A.*, 2023, **120**, e2310131120.
28. D. Calabria, M. Guardigli, M. Mirasoli, A. Punzo, E. Porru, M. Zangheri, P. Simoni, E. Pagnotta, L. Ugolini, L. Lazzeri, C. Caliceti and A. Roda, *Anal. Biochem.*, 2020, **600**, 113760.



- 1
2
3
4
5
6
7
8
9
10
11
12
13
14
15
16
17
18
19
20
21
22
23
24
25
26
27
28
29
30
31
32
33
34
35
36
37
38
39
40
41
42
43
44
45
46
47
48
49
50
51
52
53
54
55
56
57
58
59
60
29. C. Bourlieu, T. Astruc, S. Barbe, J.-G. Berrin, E. Bonnin, R. Boutrou, V. Hugouvieux, S. Le Feunteun and G. Paës, *Biotechnol. Adv.*, 2020, **41**, 107546. View Article Online
DOI: 10.1039/D4AN01082E
30. J. S. Sidhu, N. Kaur and N. Singh, *Biosens. Bioelectron.*, 2021, **191**, 113441.
31. M. R. Bond and J. A. Hanover, *Annu Rev Nutr*, 2013, **33**, 205-229.
32. R. Gupta, R. K. Ambasta and P. Kumar, *Life Sci.*, 2020, **243**, 117278.
33. J. Zhang, X. Chai, X.-P. He, H.-J. Kim, J. Yoon and H. Tian, *Chem. Soc. Rev.*, 2019, **48**, 683-722.
34. M. David, Q. Jaber, M. Fridman and D. Shabat, *Chem. - Eur. J.*, 2023, **29**, e202300422.
35. H. N. Kagalwala, R. T. Reeves and A. R. Lippert, *Curr. Opin. Chem. Biol.*, 2022, **68**, 102134.
36. A. P. Schaap, R. S. Handley and B. P. Giri, *Tetrahedron Lett.*, 1987, **28**, 935-938.
37. A. P. Schaap, T.-S. Chen, R. S. Handley, R. DeSilva and B. P. Giri, *Tetrahedron Lett.*, 1987, **28**, 1155-1158.
38. A. P. Schaap, M. D. Sandison and R. S. Handley, *Tetrahedron Lett.*, 1987, **28**, 1159-1162.
39. S. Gutkin, S. Gandhesiri, A. Brik and D. Shabat, *Bioconjugate Chem.*, 2021, **32**, 2141-2147.
40. L. Liu and R. P. Mason, *PLOS ONE*, 2010, **5**, e12024.
41. J. Cao, R. Lopez, J. M. Thacker, J. Y. Moon, C. Jiang, S. N. S. Morris, J. H. Bauer, P. Tao, R. P. Mason and A. R. Lippert, *Chem. Sci.*, 2015, **6**, 1979-1985.
42. J. Cao, J. Campbell, L. Liu, R. P. Mason and A. R. Lippert, *Anal. Chem.*, 2016, **88**, 4995-5002.
43. S. Gutkin, R. Tannous, Q. Jaber, M. Fridman and D. Shabat, *Chem Sci*, 2023, **14**, 6953-6962.
44. S. Gutkin, R. Tannous, Q. Jaber, M. Fridman and D. Shabat, *Chem. Sci.*, 2023, **14**, 6953-6962.
45. A. Fu, Y. Mao, H. Wang and Z. Cao, *J. Pharm. Biomed. Anal.*, 2021, **204**, 114266.
46. J. C. Hummelen, T. M. Luider and H. Wynberg, in *Methods Enzymol.*, Academic Press, 1986, vol. 133, pp. 531-557.
47. L. F. M. L. Ciscato, F. H. Bartoloni, A. S. Colavite, D. Weiss, R. Beckert and S. Schramm, *Photochem. Photobiol. Sci.*, 2014, **13**, 32-37.
48. M. Yang, J. Zhang, D. Shabat, J. Fan and X. Peng, *ACS Sens.*, 2020, **5**, 3158-3164.
49. K. J. Bruemmer, O. Green, T. A. Su, D. Shabat and C. J. Chang, *Angew. Chem.*, 2018, **130**, 7630-7634.
50. M. Vacher, I. Fdez. Galván, B.-W. Ding, S. Schramm, R. Berraud-Pache, P. Naumov, N. Ferré, Y.-J. Liu, I. Navizet, D. Roca-Sanjuán, W. J. Baader and R. Lindh, *Chem. Rev.*, 2018, **118**, 6927-6974.
51. W. Adam, I. Bronstein, A. V. Trofimov and R. F. Vasil'ev, *J. Am. Chem. Soc.*, 1999, **121**, 958-961.
52. L. F. M. L. Ciscato, F. H. Bartoloni, D. Weiss, R. Beckert and W. J. Baader, *J. Org. Chem.*, 2010, **75**, 6574-6580.
53. H. Takakura, *Molecules*, 2021, **26**, 1618.
54. P. Farahani, M. A. Oliveira, I. F. Galván and W. J. Baader, *RSC Adv.*, 2017, **7**, 17462-17472.
55. C. Dodeigne, L. Thunus and R. Lejeune, *Talanta*, 2000, **51**, 415-439.
56. I. Bronstein, B. Edwards and J. C. Voyta, *J. Biolumin. Chemilumin.*, 1989, **4**, 99-111.
57. Y. Hisamatsu, T. Fukiage, K. Honma, A. G. Balia, N. Umezawa, N. Kato and T. Higuchi, *Org. Lett.*, 2019, **21**, 1258-1262.
58. J. Huang, P. Cheng, C. Xu, S. S. Liew, S. He, Y. Zhang and K. Pu, *Angew. Chem. Int. Ed.*, 2022, **61**, e202203235.
59. O. Green, T. Eilon, N. Hananya, S. Gutkin, C. R. Bauer and D. Shabat, *ACS Cent. Sci.*, 2017, **3**, 349-358.
60. N. Hananya, J. P. Reid, O. Green, M. S. Sigman and D. Shabat, *Chem. Sci.*, 2019, **10**, 1380-1385.
61. O. Green, S. Gnaim, R. Blau, A. Eldar-Boock, R. Satchi-Fainaro and D. Shabat, *J. Am. Chem. Soc.*, 2017, **139**, 13243-13248.
62. J. Huang, Y. Jiang, J. Li, J. Huang and K. Pu, *Angew. Chem. Int. Ed.*, 2021, **60**, 3999-4003.
63. X. Wei, J. Huang, C. Zhang, C. Xu, K. Pu and Y. Zhang, *Angew. Chem. Int. Ed.*, 2023, **62**, e202213791.
64. G. Blum, G. von Degenfeld, M. J. Merchant, H. M. Blau and M. Bogoy, *Nat. Chem. Biol.*, 2007, **3**, 668-677.



- 1
2
3
4
5
6
7
8
9
10
11
12
13
14
15
16
17
18
19
20
21
22
23
24
25
26
27
28
29
30
31
32
33
34
35
36
37
38
39
40
41
42
43
44
45
46
47
48
49
50
51
52
53
54
55
56
57
58
59
60
65. E. A. Mason, R. Lopez and R. P. Mason, *Opt. Mater. Express*, 2016, **6**, 1384-1392. [View Article Online](#)
66. A. A. Fitzgerald and L. M. Weiner, *Cancer Metastasis Rev*, 2020, **39**, 783-803. [DOI: 10.1039/D4AN01082E](#)
67. Z. Yu, Y. Huang, H. Chen, Z. Jiang, C. Li, Y. Xie, Z. Li, X. Cheng, Y. Liu, S. Li, Y. Liang and Z. Wu, *ACS Pharmacol. Transl. Sci.*, 2023, **6**, 1745-1757.
68. L. Zhang, W. Ying, Z. Sheng, L. Lv, J. Gao, Y. Xue and L. Liu, *Anal. Biochem.*, 2022, **655**, 114859.
69. K. Dienus, A. Bayat, B. F. Gilmore and O. Seifert, *Arch Dermatol Res*, 2010, **302**, 725-731.
70. A. Fu, H. Wang, T. Huo, X. Li, W. Fu, R. Huang and Z. Cao, *Anal. Chem.*, 2021, **93**, 6501-6507.
71. J. I. Scott, S. Gutkin, O. Green, E. J. Thompson, T. Kitamura, D. Shabat and M. Vendrell, *Angew. Chem. Int. Ed.*, 2021, **60**, 5699-5703.
72. I. Voskoboinik, J. C. Whisstock and J. A. Trapani, *Nat. Rev. Immunol.*, 2015, **15**, 388-400.
73. J. A. Trapani, *Genome Biol*, 2001, **2**, Reviews3014.
74. J. E. Davis, V. R. Sutton, M. J. Smyth and J. A. Trapani, *Cell Death Differ.*, 2000, **7**, 973-983.
75. S. A. Amin, N. Adhikari and T. Jha, *J. Med. Chem.*, 2018, **61**, 6468-6490.
76. A. J. Turner, *Membrane alanyl aminopeptidase*, Handbook of Proteolytic Enzymes. 2004:289-94. doi: 10.1016/B978-0-12-079611-3.50077-X. Epub 2012 Dec 2.
77. M. Alfalah, M. P. Krahn, G. Wetzel, S. von Hörsten, C. Wolke, N. Hooper, T. Kalinski, S. Krueger, H. Y. Naim and U. Lendeckel, *J. Biol. Chem.*, 2006, **281**, 11894-11900.
78. S.-X. Cui, X.-J. Qu, Z.-H. Gao, Y.-S. Zhang, X.-F. Zhang, C.-R. Zhao, W.-F. Xu, Q.-B. Li and J.-X. Han, *Cancer Lett.*, 2010, **292**, 153-162.
79. X. Shi, Y. Deng, X. Liu, G. Gao, R. Wang and G. Liang, *Biosens. Bioelectron.*, 2022, **208**, 114212.
80. Y. Liu, J. Zeng, Q. Li, M. Miao, Z. Song, M. Zhao, Q. Miao and M. Gao, *Adv. Opt. Mater.*, 2022, **10**, 2102709.
81. R. Sun, X. Wu, Y. Mao, H. Wang, C. Bian, P. Lv, Z. Zhao, X. Li, W. Fu, J. Lu and Z. Cao, *Luminescence*, 2022, **37**, 1335-1342.
82. M. B. Harbut, G. Velmourougane, S. Dalal, G. Reiss, J. C. Whisstock, O. Onder, D. Brisson, S. McGowan, M. Klemba and D. C. Greenbaum, *Proc Natl Acad Sci U S A*, 2011, **108**, E526-534.
83. B. Wang, Z. Chen, X. Cen, Y. Liang, L. Tan, E. Liang, L. Zheng, Y. Zheng, Z. Zhan and K. Cheng, *Chem. Sci.*, 2022, **13**, 2324-2330.
84. M. J. Ahrens, P. A. Bertin, E. F. Vonesh, T. J. Meade, W. J. Catalona and D. Georganopoulou, *The Prostate*, 2013, **73**, 1731-1737.
85. A. P. Drabovich, P. Saraon, K. Jarvi and E. P. Diamandis, *Nat. Rev. Urol.*, 2014, **11**, 278-288.
86. P. Suttipapit and S. Wongwittayapanich, *J Forensic Leg Med*, 2018, **54**, 102-108.
87. S. Gutkin, O. Green, G. Raviv, D. Shabat and O. Portnoy, *Bioconjugate Chem.*, 2020, **31**, 2488-2493.
88. V. Turk, V. Stoka, O. Vasiljeva, M. Renko, T. Sun, B. Turk and D. Turk, *Biochim. Biophys. Acta - Proteins Proteom.*, 2012, **1824**, 68-88.
89. M. C. Yoon, V. Hook and A. J. O'Donoghue, *Biochemistry*, 2022, **61**, 1904-1914.
90. T. R. Lambeth, Z. Dai, Y. Zhang and R. R. Julian, *RSC Chem. Biol.*, 2021, **2**, 606-611.
91. A. Amritraj, K. Peake, A. Kodam, C. Salio, A. Merighi, J. E. Vance and S. Kar, *Am J Pathol.*, 2009, **175**, 2540-2556.
92. H. Dong, Y. Qin, Y. Huang, D. Ji and F. Wu, *Neurochem. Int.*, 2019, **126**, 178-186.
93. K. Ditaranto, T. L. Tekirian and A. J. Yang, *Neurobiol. Dis.*, 2001, **8**, 19-31.
94. M. E. Roth-Konforti, C. R. Bauer and D. Shabat, *Angew. Chem. Int. Ed.*, 2017, **56**, 15633-15638.
95. J. M. Harris and R. B. Chess, *Nat. Rev. Drug Discov.*, 2003, **2**, 214-221.
96. J. A. Hoffman, E. Giraud, M. Singh, L. Zhang, M. Inoue, K. Porkka, D. Hanahan and E. Ruoslahti, *Cancer Cell*, 2003, **4**, 383-391.
97. M. E. Roth-Konforti, C. R. Bauer and D. Shabat, *Angew. Chem. Int. Ed. Engl.*, 2017, **56**, 15633-15638.
98. S. Chen, X. Ma, L. Wang, Y. Wu, Y. Wang, W. Fan and S. Hou, *Sens. Actuators B: Chem.*, 2023, **379**, 133272.
99. A. T. Hoogeveen, F. W. Verheijen and H. Galjaard, *J. Biol. Chem.*, 1983, **258**, 12143-12146.



- 1
2
3
4
5
6
7
8
9
10
11
12
13
14
15
16
17
18
19
20
21
22
23
24
25
26
27
28
29
30
31
32
33
34
35
36
37
38
39
40
41
42
43
44
45
46
47
48
49
50
51
52
53
54
55
56
57
58
59
60
100. S. Zhang, J. McCarter, Y. Okamura-Oho, F. Yaghi, A. Hinek, S. Withers and J. Callahan, *Biochem. J.*, 1994, **304**, 281-288. View Article Online
DOI: 10.1039/94AN01082E
101. M. Li, M. Yang and W.-H. Zhu, *Mater. Chem. Front.*, 2021, **5**, 763-774.
102. D. Asanuma, M. Sakabe, M. Kamiya, K. Yamamoto, J. Hiratake, M. Ogawa, N. Kosaka, P. L. Choyke, T. Nagano, H. Kobayashi and Y. Urano, *Nat. Commun.*, 2015, **6**, 6463.
103. J. Zhang, P. Cheng and K. Pu, *Bioconjugate Chem.*, 2019, **30**, 2089-2101.
104. J. Y. Park, J. Gunpat, L. Liu, B. Edwards, A. Christie, X.-J. Xie, L. J. Kricka and R. P. Mason, *Luminescence*, 2014, **29**, 553-558.
105. J.-C. Tseng and A. L. Kung, *J. Biomed. Sci.*, 2015, **22**, 45.
106. N. Hananya, A. Eldar Boock, C. R. Bauer, R. Satchi-Fainaro and D. Shabat, *J. Am. Chem. Soc.*, 2016, **138**, 13438-13446.
107. J. Zalejski, J. Sun and A. Sharma, *J Imaging*, 2023, **9**.
108. F. Zheng, W. Xiong, S. Sun, P. Zhang and J. J. Zhu, *Nanophotonics*, 2019, **8**, 391-413.
109. T. Eilon-Shaffer, M. Roth-Konforti, A. Eldar-Boock, R. Satchi-Fainaro and D. Shabat, *Org. Biomol. Chem.*, 2018, **16**, 1708-1712.
110. L. J. van 't Veer and R. Bernards, *Nature*, 2008, **452**, 564-570.
111. R. N. Woodring, E. G. Gurysh, E. M. Bachelder and K. M. Ainslie, *ACS Applied Bio Materials*, 2023, **6**, 934-950.
112. M. I. Khan, M. I. Hossain, M. K. Hossain, M. H. K. Rubel, K. M. Hossain, A. M. U. B. Mahfuz and M. I. Anik, *ACS Applied Bio Materials*, 2022, **5**, 971-1012.
113. S. Gnaim, A. Scomparin, S. Das, R. Blau, R. Satchi-Fainaro and D. Shabat, *Angew. Chem. Int. Ed.*, 2018, **57**, 9033-9037.
114. L. Feng, Z. M. Liu, J. Hou, X. Lv, J. Ning, G. B. Ge, J. N. Cui and L. Yang, *Biosens. Bioelectron.*, 2015, **65**, 9-15.
115. S. F. Sousa, M. J. Ramos, C. Lim and P. A. Fernandes, *ACS Catal.*, 2015, **5**, 5877-5887.
116. C. Morisseau, *Int J Mol Sci*, 2022, **23**.
117. F. Wang, Y. Wang, J. Zhang, S. Zheng, B. Xie, S. Lu, J. Zhou, C. Wang, F. Wang, M. Jiang and X. Chen, *Sens. Actuators B: Chem.*, 2023, **375**, 132880.
118. X. Liu, S. Zeng, M. Zhang, M. Jiang, Y. S. Kafuti, P. Shangguan, Y. Yu, Q. Chen, J. Wang, X. Peng, J. Yoon and H. Li, *Chem. Commun.*, 2022, **58**, 11438-11441.
119. C. Weng, H. Yang, B. S. Loh, M. W. Wong and W. H. Ang, *J. Am. Chem. Soc.*, 2023, **145**, 6453-6461.
120. Elsie M. Williams, Rory F. Little, Alexandra M. Mowday, Michelle H. Rich, Jasmine V. E. Chan-Hyams, Janine N. Copp, Jeff B. Smaill, Adam V. Patterson and David F. Ackerley, *Biochem. J.*, 2015, **471**, 131-153.
121. D. Liu, T. N. Wanniarachchi, G. Jiang, G. Seabra, S. Cao, S. D. Bruner and Y. Ding, *RSC Chem. Biol.*, 2022, **3**, 436-446.
122. R. S. Boddu, O. Perumal and D. K, *Biotechnol. Appl. Biochem.*, 2021, **68**, 1518-1530.
123. W. Wang, J. Cai, N.-K. Wong, M. Hong, J. Deng, L. Jin, Y. Ran, Y. Zhang, Y. Zhou and B.-O. Guan, *Analyst*, 2022, **147**, 1449-1456.
124. A. Chevalier, Y. Zhang, O. M. Khmour, J. B. Kaye and S. M. Hecht, *J. Am. Chem. Soc.*, 2016, **138**, 12009-12012.
125. S. A. Yoon, J. Chun, C. Kang and M. H. Lee, *ACS Applied Bio Materials*, 2021, **4**, 2052-2057.
126. W. Sun, M. Tong, G. Liu, X. Wang, N. Fan, X. Song, D. Yang and D. Zhang, *Results Chem.*, 2021, **3**, 100177.
127. R. Tannous, O. Shelef, S. Gutkin, M. David, T. Leirikh, L. Ge, Q. Jaber, Q. Zhou, P. Ma, M. Fridman, U. Spitz, K. N. Houk and D. Shabat, *ACS Cent. Sci.*, 2024, **10**, 28-42.
128. J. Sun, Z. Hu, R. Wang, S. Zhang and X. Zhang, *Anal. Chem.*, 2019, **91**, 1384-1390.
129. L. S. Ryan, J. Gerberich, J. Cao, W. An, B. A. Jenkins, R. P. Mason and A. R. Lippert, *ACS Sens.*, 2019, **4**, 1391-1398.
130. A. L. Pey, C. F. Megarity and D. J. Timson, *Biosci. Rep.*, 2019, **39**.

- 1
2
3
4
5
6
7
8
9
10
11
12
13
14
15
16
17
18
19
20
21
22
23
24
25
26
27
28
29
30
31
32
33
34
35
36
37
38
39
40
41
42
43
44
45
46
47
48
49
50
51
52
53
54
55
56
57
58
59
60
131. M. Faig, M. A. Bianchet, P. Talalay, S. Chen, S. Winski, D. Ross and L. M. Amzel, *Proc. Natl. Acad. Sci. U. S. A.*, 2000, **97**, 3177-3182. View Article Online
DOI: 10.1039/D4AN01082E
132. S. R. Punganuru, H. R. Madala, V. Arutla, R. Zhang and K. S. Srivenugopal, *Sci. Rep.*, 2019, **9**, 8577.
133. S. Son, M. Won, O. Green, N. Hananya, A. Sharma, Y. Jeon, J. H. Kwak, J. L. Sessler, D. Shabat and J. S. Kim, *Angew. Chem. Int. Ed.*, 2019, **58**, 1739-1743.
134. S. R. Pinnell and G. R. Martin, *Proc. Natl. Acad. Sci. U. S. A.*, 1968, **61**, 708-716.
135. S. D. Vallet, M. Guéroult, N. Belloy, M. Dauchez and S. Ricard-Blum, *ACS Omega*, 2019, **4**, 8495-8505.
136. T. Liburkin-Dan, S. Toledano and G. Neufeld, *Int. J. Mol. Sci.*, 2022, **23**, 6249.
137. L. Leung, D. Niculescu-Duvaz, D. Smithen, F. Lopes, C. Callens, R. McLeary, G. Saturno, L. Davies, M. Aljarah, M. Brown, L. Johnson, A. Zambon, T. Chambers, D. Ménard, N. Bayliss, R. Knight, L. Fish, R. Lawrence, M. Challinor, H. Tang, R. Marais and C. Springer, *J. Med. Chem.*, 2019, **62**, 5863-5884.
138. J. Huang, C. Zhang, X. Wang, X. Wei and K. Pu, *Angew. Chem. Int. Ed.*, 2023, **62**, e202303982.
139. R. J. Obaid, E. U. Mughal, N. Naeem, A. Sadiq, R. I. Alsantali, R. S. Jassas, Z. Moussa and S. A. Ahmed, *RSC Adv.*, 2021, **11**, 22159-22198.
140. T.-S. Chang, *Materials*, 2012, **5**, 1661-1685.
141. O. Shelef, A. C. Sedgwick, S. Pozzi, O. Green, R. Satchi-Fainaro, D. Shabat and J. L. Sessler, *Chem. Commun.*, 2021, **57**, 11386-11389.
142. M. H. Hanigan, in *Advances in Cancer Research*, eds. D. M. Townsend and K. D. Tew, Academic Press, 2014, vol. 122, pp. 103-141.
143. P. N. Brennan, J. F. Dillon and E. B. Tapper, *Liver International*, 2022, **42**, 9-15.
144. M. B. West, Y. Chen, S. Wickham, A. Heroux, K. Cahill, M. H. Hanigan and B. H. M. Mooers, *J. Biol. Chem.*, 2013, **288**, 31902-31913.
145. R. An, S. Wei, Z. Huang, F. Liu and D. Ye, *Anal. Chem.*, 2019, **91**, 13639-13646.

Phenoxy-1,2-dioxetane-Based Activatable Chemiluminescent Probes: Tuning of Photophysical Properties for Tracing Enzymatic Activities in Living Cells

Jagpreet Singh Sidhu^{a*}, Gurjot Kaur^b, Atharva Rajesh Chavan^a and Rajeev Taliyan^a

^a Department of Pharmacy, Birla Institute of Technology and Science Pilani, Pilani Campus, Rajasthan, 333031, India

^b Khalsa College Amritsar, Punjab, 143002, India

*Email: jagpreet.sidhu@pilani.bits-pilani.ac.in

Data Availability

No primary research results, software or code have been included and no new data were generated or analysed as part of this review.

1
2
3
4
5
6
7
8
9
10
11
12
13
14
15
16
17
18
19
20
21
22
23
24
25
26
27
28
29
30
31
32
33
34
35
36
37
38
39
40
41
42
43
44
45
46
47
48
49
50
51
52
53
54
55
56
57
58
59
60

Analyst Accepted Manuscript

